Distribution Agreement

In presenting this thesis or dissertation as a partial fulfillment of the requirements for an advanced degree from Emory University, I hereby grant to Emory University and its agents the non-exclusive license to archive, make accessible, and display my thesis or dissertation in whole or in part in all forms of media, now or hereafter known, including display on the world wide web. I understand that I may select some access restrictions as part of the online submission of this thesis or dissertation. I retain all ownership rights to the copyright of the thesis or dissertation. I also retain the right to use in future works (such as articles or books) all or part of this thesis or dissertation.

Signature:

Shijian Jin	Date

Synthesis and Excited State Dynamics of Oligothiophene-Nitronyl Nitroxides

By

Shijian Jin
Master of Science
Chemistry

Eilaf Egap, Ph.D
Advisor

Dr. Craig L. Hill, Ph.D
Committee Member

Dr. Huw M. L. Davies, Ph.D
Committee Member

Accepted:

Lisa A. Tedesco, Ph.D
Dean of the James T. Laney School of Graduate Studies

Date

Synthesis and Excited State Dynamics of Oligothiophene-Nitronyl Nitroxides

By

Shijian Jin

Advisor: Eilaf Egap, Ph.D

An abstract of
A dissertation submitted to the Faculty of the
James T. Laney School of Graduate Studies of Emory University
in partial fulfillment of the requirements for the degree of
Master of Science
in Chemistry
2017

Abstract

Synthesis and Excited State Dynamics of Oligothiophene-Nitronyl Nitroxides

By Shijian Jin

Spin-electronics or spintronics are envisioned to have faster data processing and accessing capabilities and higher information storage density compared to traditional electronics due to their intrinsic spin properties. Currently, the field of spintronics is dominated by silicon-metal multilayer materials. Recently, organic-based materials, particularly pi-conjugated chromophores and persistent radicals, have been of interest due to their metal-like spin properties, photo-controllable spin states, structural flexibility, low-cost, and Eco-friendly manufacturing processibility. However, low charge carrier mobility, weak ferromagnetism, and marginal understanding of the spin-dynamics in organic radicals have limited their applications. Oligothiophene-based radicals represent an attractive alternative and may potentially address these challenges because of the high carrier mobility observed in oligothiophenes (0.6 $cm^2V^{-1}s^{-1}$). Furthermore, photoexcitation of oligothiophenes generate large population of long-living triplet state via intersystem crossing, where the spins are aligned, which infer potential ferromagnetic properties of oligothiophenes-radicals. This thesis presents and elaborates on the synthesis and spectroscopic studies of oligothiophene-nitronyl nitroxide (OT-NN) radicals. The crystal structure, packing pattern and steady-state magnetic properties of bithiophene-bis(nitronyl nitroxide) (1.4) are also studied. Electronic coupling as well as the presence of unpaired spins have completely changed the electronic structure. Computational and experimental approaches both prove that the existence of radical components in OTNN lower the bandgap through electronic coupling. Several new n-π^* induced low-lying charge-transfer states are also present in the OTNN system. The possible post-photoexication spin transitions are analyzed using ultrafast transient absorption.

Synthesis and Excited State Dynamics of Oligothiophene-Nitronyl Nitroxides

By

Shijian Jin

Advisor: Eilaf Egap, Ph.D

A dissertation submitted to the Faculty of the
James T. Laney School of Graduate Studies of Emory University
in partial fulfillment of the requirements for the degree of
Master of Science
in Chemistry
2017

Acknowledgement

I would like to thank my research advisor, Dr. Eilaf Egap for her guidance on my research, writing, and life in general. She has always been a helpful and encouraging advisor. Her advice and critiques have helped me develop important research skills.

I would like to thank my academic advisor and committee member Dr. Huw Davies. Dr. Davies has been my academic advisor since my freshmen year, and he has always been resourceful. He has given me the opportunity to conduct research in the Itami lab, which has greatly strengthened my interests in research.

I would like to thank my committee member Dr. Craig Hill. Dr. Hill has not only given suggestions on my research but also broadened my view in energy sciences, material sciences and chemistry in general. I have always enjoyed the inspiring talks at his office, as well as during classes.

I would like to thank Dr. Tim Lian, Dr. Francesco Evangelista, Dr. Kurt Warncke and Zihao Xu for their generous help on my research.

I would like to thank all of my professors and lecturers in the Department of Chemistry, as well as other Departments, for the knowledge and life experience I gained in their classrooms.

I appreciate the help of Dr. Shaoxiong Wu and Dr. Bing Wang at Emory's NMR Center, Dr. John Bacsa at the X-ray Crystallography Center, the staff at the MS-Spec Center, Steve and Claire in the chemistry stockroom, and Mrs. Ann Dasher.

I am grateful to Dr. Yiming Huang, who has been a great mentor and a dear friend to me. Yiming has given me substantial advice on organic synthesis, spectroscopy, quantum physics, as well as writing and software usage. He has never been annoyed by my incessant questions and has always been willing to explain things to me. Because of this, he has helped me progress much faster. Thank you so much!

I want to express my thankfulness to Dr. Yiming Huang, Dr. Karimulla Mulla, Jiahui Zhang, Zhe Su, Yifan Zhu, Shelly Saini and Yulei Cao. They have always been friendly, helpful and encouraging lab members. The three years I spent in the Egap lab have been and always will be precious to me.

Finally, I want to thank my parents, who have always been supportive of me in all aspects of life. I wouldn't have achieved anything without them.

Table of Contents

List of Figures

List of Tables

List of Schemes

Chapter 1 Synthesis and Excited State Dynamics of Oligothiophene-Nitronyl Nitroxides

1.1 Introduction

1.1.1 Spintronics

Traditional electronics utilize the electrical energy of electrons, while latest spintronics, or spinelectronics, employ the other important intrinsic property - the spin of electrons and the associated magnetic moments.[1–3] Since the two-way, i.e. $+\frac{1}{2}$ or $-\frac{1}{2}$, spin angular momentum resembles the binary code of a computer, spintronics have been applied in computer memory devices such as magnetoresistive random-access memory (MRAM) and solid state drive (SSD).[2] In addition, the increased degree of freedom in addition to electron charge due to the exploitation of spin properties, spintronics are advantageous in terms of fast data reading and accessing, and reduced calculation time.[4] Currently, the most commonly applied spintronics, i.e. hard drive read head or MRAM, adopt a multilayer structure that consists of alternating ferromagnetic and diamagnetic sheets.[5] Upon the application of an external magnetic field, the electron spins in the magnetic sheets either align or anti-align with the direction of the field. While there is an unequal distribution of the spin directions, a bulk magnetization is formed, which also induces a change in resistance.[6] The magnetization-induced change in resistance is caused by the giant magnetoresistance effect (GMR). To maximize the GMR effect, one must devise a system that can retain unevenly populated spins for an extended period and allow fast electron/spin transport.[7]

There have been large applications as well as research on metal-based spintron-

ics.[5,8,9] Xiang et al. fabricated Fe_3O_4 thin films with tunable magnetic properties on silver-buffered one-dimensional silicon, and they found the oxidized Fe_3O_4 layer and the elemental Fe both contributed to magnetic properties of the material but had different effects.[8] Therefore, the magnetic properties could be tuned through controlling the annealing time.[8] Ueda et al. discovered carrier-induced ferromagnetism in cobalt-doped ZnO thin films, whose magnetic properties depend on cobalt ion and carrier concentration.[10]

1.1.2 Organic Radicals

As potential alternatives to costly and environmental unfriendly metal materials, organic radicals draw the attention of researchers due to their ferromagnetic properties that resemble metal materials. Also, organic structures are more tunable structures than metal materials.[3] A common organic radical consists of a conjugated π-system chromophore center and a covalently linked radical, such as tert-butylphenyl nitroxide (BPNO), nitronyl nitroxide (NN), iminyl nitroxide (IN) and (2,2,6,6-Tetramethylpiperidin-1-yl)oxyl (TEMPO). Thermodynamics and spin properties of the organic radicals can be altered by managing the topology with structural modifications to change the distance and position of the radical with respect to the chromophore. Giacobbe et al. revealed that the insertion of a phenyl spacer in between BPNO radical and perylene-3,4:9,10-bis(dicarboximide) (PDI) would increase the lifetime of triplet excited state of PDI by an order of magnitude while decrease the triplet quantum yield by half.[11] The extended triplet lifetime(τ_{T}) is beneficiary for potential spintronic applications because all spins are aligned in the triplet state; both of spin alignment, which generates ferromagnetic property, and the lifetime of aligned spins are vital to spintronics. Stability, another important factor to spintronics and all other electronics, of organic material may also be enhanced by introducing the radical system. Pentacene, a conventional but air and light sensitive p-type or-

ganic semiconductor is stabilized through the installation of two phenyl NN radicals at 6 and 13 carbons.[12] Kawanaka et al. improved the photostability of pentacene as a result of radical-facilitated quick relaxation of the unstable excited electronic states of pentacene.[12]

Besides the effect of the change in geometric structure, photoexcitation-induced change of electronic structure also creates different spin properties.[13] And the presence of radical influences the spin geometry in excited states and may create spin-aligned states with prolonged lifetime. For a typical nonradical organic molecule with π-conjugated structure, an electron/spin on the highest occupied molecular orbital (HOMO), is promoted to the lowest unoccupied molecular orbital (LUMO), forming a singlet excited state (Figure 1.1). The excited molecule then returns to ground state through one of the three mechanisms, fluorescence, translational/vibrational relaxation, a.k.a. internal conversion (IC), and intersystem crossing (ISC). Fluorescence is the only type of radiative decay of singlet excited state, featuring the release of a photon. The number of the electrons returning to ground state through fluorescence is documented as fluorescence quantum yield Φ_{F}. IC and ISC are nonradioactive decays because no photon is released during either process. IC describes energy release through collisions, movement, vibrations and rotations of molecules. ISC takes place when the spin on one of the two electronic states flips and generates a triplet state with all spins aligned, which is lower in energy, according to Hund's rule. The triplet state has a long lifetime (usually in the microseconds) because the spin transition from triplet state to ground state, another type of ISC, is a spin-forbidden process. The triplet formation as well as triplet quantum yield, Φ_{T}, depends on spin-orbit coupling, the proximity of the triplet state energy level to excited singlet state energy level and the energy difference. Researchers in fields of energy science and engineers designing energy-harvesting materials favor triplet-generating molecules because they can harvest energy from the long-living triplet state.

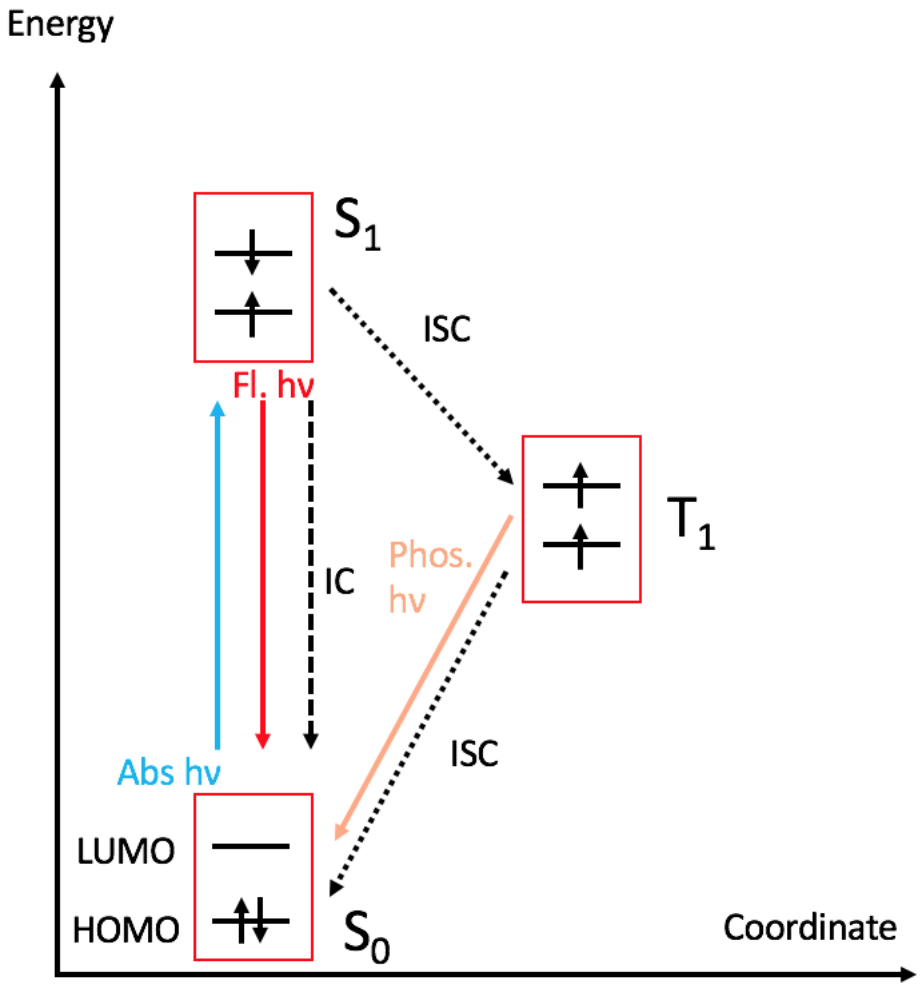

Figure 1.1: Electronic transitions in a typical conjugated chromophore. Abs, fl, phos IC, ISC refer to absorption, fluorescence, phosphorescence, internal conversion and intersystem crossing, respectively.

Molecules with long-living spin aligned states are suitable materials for organic spintronics because of their magnetic properties. The addition of a radical to an organic chromophore is considered as one of the methods the increase Φ_T and accelerates triplet formation.[11] When a radical is linked to an organic chromophore, new electronic states, as well as an unpaired electron, is introduced into the system, and thus new state geometries are formed. Photoexcitation of such chromophore-radical system results in much more complicated transitions, which will be elaborated in the next paragraph. Much work has shown that photoexcitation generates significant difference between the magnetic properties of organic radicals at ground state and excited state.To date, excited state magnetic properties of stable radicals covalently linked to aromatic chromophores were discussed, including phthalocyanine,[14] pentacene,[14,15] and perylenediimide.[11,16]

Most organic radicals that consist of chromophore-radical structure have extremely low Φ_F due to the multiple additional spin pathways that the radical part brings to the system. Major pathways that may contribute to the fluorescence quenching include:(1) Förster/Dexter energy transfer, (2) electron transfer, (3) electron-exchange enhanced intersystem crossing (EISC) and (4) enhanced internal conversion (EIC), where the most common cases are the latter two.[11] Förster/Dexter energy transfers require an overlap between the fluorescence of the chromophore and the absorption of the radical. Dexter energy transfer is useful in photon upconversion within quantum dot related systems but a rare case in organic chromophore-radicals. Förster energy transfer is more often applied in biochemically related macromolecules. Several groups reported fluorescence quenching by intermolecular electron transfer while only Green et al. discovered fluorescence quenching by intramolecular charge transfer in the 1,4,5,8-naphthalene-bis(dicarboximide) (NDI)-TEMPO system.[11,17] Green et al. observed triplet quenching by the same mechanism, as well as a long-lived (200 μs) charge separation state.[17] The researchers found the long-lived charge-separation

state was caused by the rigid geometry of $NDI^{-}TEMPO^{+}$ system that limited back electron transfer, i.e. electron transferring from the negatively charged NDI to positively charged TEMPO and making both parts neutral. However, due to the low resolution of the transient absorption technique they were using, the authors were unable to ascertain the presence nor the lifetime of a triplet state.[17] Giacobbe et al. and Colvin et al. suggested an extended (τ_T) and (Φ_T) by EISC in PDI-radical systems.[11,16] Giacobbe, Colvin and Green all argued that the orientation of the system and the distance between radical and chromophore are critical to the electronic transitions. EIC is the mechanism where the energy release through vibration or rotation among molecules is expedited by the presence of radical. IC is a very fast and thus undesired process. Many groups have reported that the installation of radical to an organic chromophore enhanced the internal conversion due to the additional closely packed vibrational and rotational states introduced by the radical.[18,19] Electron transfer and energy transfer processes are less studied in organic radicals due to their rarity, but they are hot fields in research related to organic semiconductors and quantum dots. Many researchers in fields of energy science and material science aim to achieve EISC and avoid EIC in their organic radicals since the former is a much slower and exploitable process than the latter. Most current research about organic spintronics focuses on developing new organic radicals with different chromophores to achieve fast-forming and long-living spin-aligned states.

1.1.3 Oligo- and Poly-Thiophenes

Polythiophene is among the most desiring organic materials because of its metal-like properties such as electrical conductivity upon doping, and tunable optical properties which make polythiophenes potential candidates for organic field-effect transistors, organic light-emitting diodes, metal-/bio-sensors, etc. Armour et al. synthesized polythiophene in 1967 and measured the proton transferability of the trichloroacetic

acid-protonated polythiophene in aprotic solutions.[20] More research on the electrical properties of polythiophenes emerged in the early 1980s as the highly conductive (0.02 $\omega^1 cm^{-1}$) poly(2,5-thiophenediyl)-arsenic pentafluoride complexes were obtained.[21] The discovery of high thermal stability and low air/oxygen sensitivity of undoped and oxidants, such as $CF_3SO_3^-$, doped polythiophene and poly-3-methylthiophenes derivatives encouraged researchers to explore more potential applications of polythiophene.[22] For example, polythiophene-based color switching devices have been developed, and their kinetics studied.[23] Yoshino Katsumi and coworkers initiated many applications of polythiophene such as a fluorescent dye containing polythiophene bipolar thin film transistor with Ti/Au electrodes and Nylon coating, which shows promising effective carrier mobility and transconductance.[24] More systematic studies and device development carried out by Richard McCullough and coworkers throughout the last two decades led polythiophene-based materials a significant step forward toward applications as organic electronics and product commercialization.[25,26]

While the satisfying thermal stability and electrical conductivity of polythiophene derivatives promote their functions as organic electronic devices, the shorter oligothiophenes (OT), with the number of thiophene units (n) between two to six, possess fascinating electronic structures such as adjustable HOMO-LUMO band gap, higher HOMO energy, and singlet-triplet state proximity. Experimental data, as well as computational approaches, show that the HOMO-LUMO band gap for oligothiophenes ranges from 4.09 eV (n = 2) to 2.72 eV (n = 6) and there is a loose linearly relationship between the inversed conjugation length and the band gap.[27,28] A similar trend is also found in the relative electronic energy levels of oligothiophenes, where the dimer has a HOMO energy of 1.17 eV, tetramer 0.90 eV and hexamer 0.85 eV relative to Ag/AgCl reference electrode.[29] The variable band gap energies and HOMO energy levels make oligothiophenes desirable units in organic materials, particularly donor-acceptor type semiconductors. Thiophene oligomers of different size are often matched with accep-

tor oligomers that have suitable energy levels and band gap, to form semiconductor materials with various functions. For example, a well-studied n-type polymer semiconductor consists of bithiophene and bis(octyldodecyl)-NDI;[30] tetrathiophene acts as an electron donor in the quarterthiophene-fullerene dyad, which establishes a long-lived (μs) charge separation state after photoexcitation,[31] and the single crystal of sexithiophene (n = 6) itself is a decent material for thin film organic transistors.[32] An inverse correlation is also found in the Φ_T of oligothiophenes of different chain lengths. Becker et al. collected a series of optical data on oligothiophenes with ring number two to seven.[33] They reported that bithiophene has 99% Φ_T and a τ_T of 104 μs while heptathiophene (n = 7) has Φ_T of less than 60% and a τ_T of 21 μs; the Φ_T and the τ_T of the oligomers with ring number in between two and seven decrease accordingly as ring number increases.[33] Bithiophene has the highest triplet yield and fastest intersystem crossing rate because it has a higher triplet state, T_4, located in the same energy range as the singlet excited state S_1.[28] Such proximity of the two energy levels facilitates intersystem crossing, which is otherwise a spin-forbidden process. The τ_T of bithiophene is long because the energy gap between the lowest-energy triplet state T_1 and the ground state S_0 is rather large (1.84 eV),[28] which slows down the triplet decay.(Figure 1.2) The optical properties of bithiophene make it a potential material for organic spintronics since the latter require fast spin-polarization and long lifetime of polarized spins. Longer oligothiophenes are less desirable for long-lived triplets. As chain size extends, the energy gap between S_0 and T_1 shrinks, which accelerates triplet decay. Meanwhile, the energy gap associated with ISC from S_1 increases, which slows down triplet formation(Figure 1.2). Both changes result in decreased Φ_T, which limits long oligothiophenes and polythiophenes' applications as spintronics.[25] We aim to modify the electronic structures of these longer thiophene oligomers and make them similar to the electronic state configuration of bithiophene so that their triplet states could be more accessible via ISC. One way to achieve this

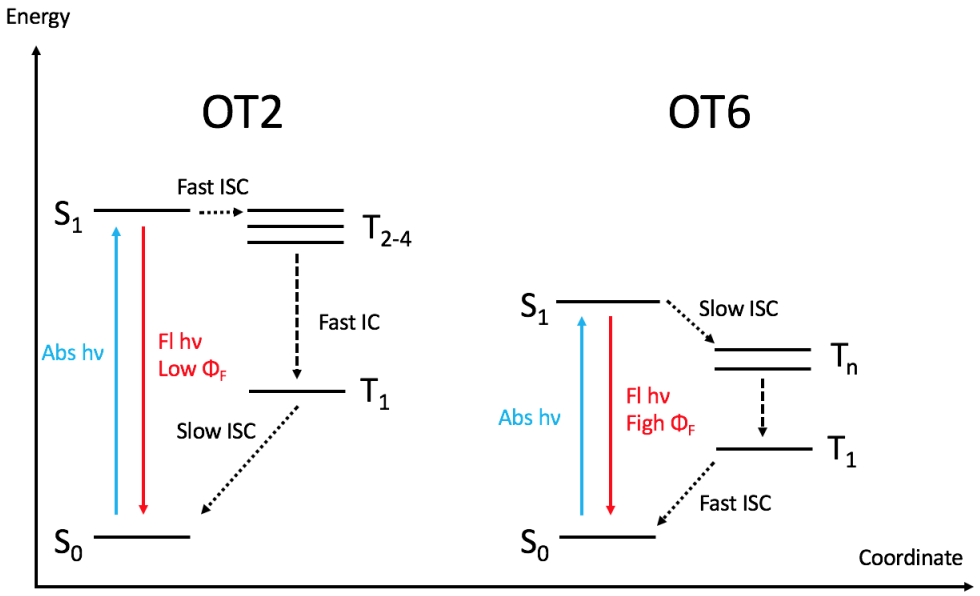

Figure 1.2: Electronic states of Bithiophene(OT2) and Sexithiophene(OT6). OT2 has high triplet yield because the gap between T_4 and S_1 is small. Also, the gap between T_1 and S_0 is large in OT2. On the other hand, OT6 has large T_n, S_1 gap and slow T_1, S_0 gap, so its triplet yield is much smaller

goal is to conjugate oligothiophene with nitroxide radicals, whose conjugation with thiophene center generates additional energy levels. These new energy levels may accelerate triplet formation if they are proximal to the singlet excited state. Triplet decay may also slow down if conjugation decreases S_0 energy or increases T_1 energy.

1.1.4 Oligothiophene-Radical

Despite the fact that oligo-/poly-thiophene derivatives are widely studied and used in organic electronics, only few research has been reported about properties of oligo-/poly-thiophene-radical systems and their spin control mechanism. Since poly-thiophene derivatives possess better charge transport ability, higher thermal stability, higher melting point and lower viscosity than smaller oligothiophenes, thiophene polymers are preferred by material scientists when making devices and applications in real life. As for spintronic applications and energy harvesting materials, similarly, polythiophene-radical systems can be more advantageous for their stability

and electrical conductivity. However, only few groups have reported the application of poly(thiophene-3-TEMPO) systems as battery electrodes, and their studies emphasized more on electrochemical properties rather than optical, magnetic or spin properties, which are essential to spintronic or energy applications.[34] In fact, even studies on those properties of simpler oligothiophene-radical systems are scarce, and it is unrealistic to work on polythiophene-radical applications without developing a fundamental understanding of the smaller and simpler oligothiophene-radical system. Hiizu Iwamura's group is one of the few pioneers in thiophene-radical studies.[35] The group prepared a series of mono/dithienyl-radical pairs and presented their crystal packing pattern as well as magnetic properties under various temperature, and they concluded that dangling imino nitroxide radicals on both sides of bithiophene have little interactions due to limited spin delocalization from the radical to bithiophene. This observation implies that the system, while at ground state, is a weak coupler for aligning the attached spins.[35] However, their discovery was limited to ground state spin interactions with no more than two thiophene units involved. We targeted a series oligothiophene-based radicals, among which the OT conjugation length, radical structures, OT-radical distances and other parameters are varied. The group aims to understand the trends, such as structure-property relationship, of the OT-radical systems, and uses the knowledge in the future design of polythiophene-radical structures with optimal characteristics. This thesis elaborates on the synthesis strategy and optical, magnetic and structural properties of the first, the smallest, and thus the most fundamental molecule among the series of organic radicals, 2,2'-bithiophenyl-5,5'-dinitronyl nitroxide.(Figure 1.3) Nitronyl nitroxide (NN) offers superior thermal stability compared to other radicals such as BPNO, and it can be connected with the chromophore through π-conjugation. TEMPO is stable and available, but there is no conjugation between the radical and thiophene. Conjugation is preferred since radicals will have more influence over OT electronic states and spin transitions if an large

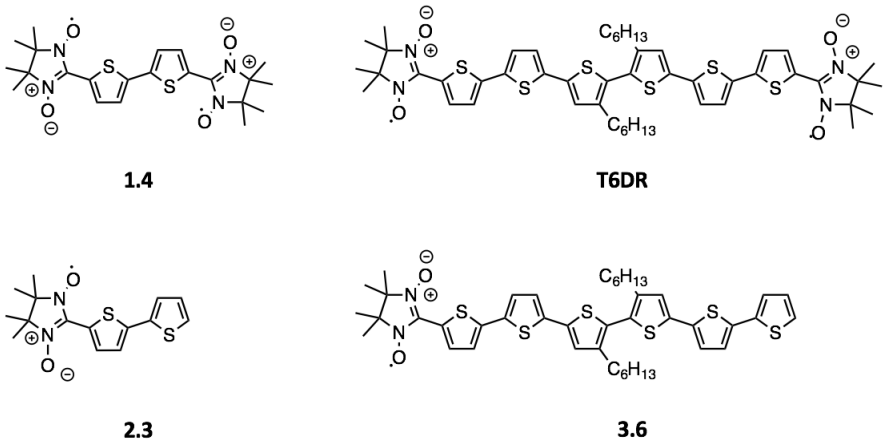

Figure 1.3: The electronic states of 1.4, T6DR and 3.6 are analyzed.

orbital-overlap occurs between OT and radical.[13] Although the Iwamura group gives a negative opinion on the thiophene-IN system, the more delocalized NN radical may behave differently, and the excited state spin properties are worthy of exploring.[35] The synthesis of bithiophene-2-mono nitronyl nitroxide (2.3) was attempted when diradical system was found to be rather complicated to interpret, but the synthesis failed to proceed, so the attempt was abandoned. Instead, a sexithiophene-NN monoradical (3.6) was synthesized with the steady-state and excited state optical properties compared with those of sexithiophene (OT6) and sexithiophene-NN diradical (T6DR).

1.2 Experimental Methods

1.2.1 General Procedure

All commercially available reagents were purchased and used without further purification. TLC plates (silica gel 60 F 254) were purchased from Merck KGaA (Darmstadt, Germany). NMR spectra were obtained on an Agilent (Santa Clara, CA) Varian VNMR 400 spectrometer operated at 400 MHz at room temperature. The steady-state optical properties of the radicals and oligothiophenes were studied with Agilent (Santa Clara, CA) Cary 60 UV-vis Spectrophotometer and Agilent Cary Eclipse Fluorometer. The fluorescence quantum yield of the radicals was measured against Rhodamine 6G in ethanol, absorbance = 0.13 350 nm; excitation wavelength was 350nm with a 2.5 nm slit width and emission was detected ranging from 360 to 700 nm with a 2.5 nm slit width. Femtosecond and nanosecond transient absorption spectroscopy (Prof. Tim Lian, Department of Chemistry) was carried out at 293 K with 400 nm excitation wavelength. A sample was prepared by dissolving target radical in toluene (100 μM) and the solution was degassed by five cycles of freeze-pump-thaw before transferred to a 1 mm path length quartz cuvette in an inert atmosphere. Mass spectra were obtained with normal electronspray ionization (ESI) method on a Thermo LTQ-FTMS using a nanospray source. Steady-state continuous wave EPR experiments (Prof. Kurt Warncke, Department of Physics) at X-band (9.5 GHz) has been conducted at 120 K on a Bruker E500 spectrometer to study the intramolecular spin-spin interactions. X-ray crystallography:

Dark green crystals of 1.4 were obtained by slow diffusion of hexanes into a dichloromethane solution of RA2. A suitable crystal was selected, and the crystal was mounted on a loop with paratone oil on a 'Bruker APEX-II CCD' diffractometer. The crystal was kept at 100±2 K during data collection. Using Olex2,[36] the structure was solved with the XT[37] structure solution program using Intrinsic Phas-

ing and refined with the XL[38] refinement package using Least Squares minimization. The images were produced with Mercury 3.8 (Build RC2), which was distributed by the Cambridge Crystallographic Data Centre.

1.2.2 Synthesis

Synthesizing 1.4

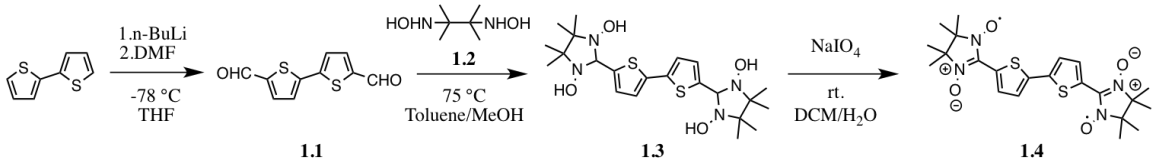

Scheme 1.1: Synthesis of 1.4

1.1 [2,2'-Bithiophene]-5,5'-dicarbaldehyde 1.1 was synthesized following a method provided by Bader et al.[39] 2,2 -bithiophene (498 mg, 3.00 mmol, 1 equiv) was dissolved in 30 mL of anhydrous THF in an oven-dried RBF. The solution was left under argon and cooled to -78 °C. A 2.5M hexanes solution of n-BuLi (4.80 mL, 12.0 mmol, 4 equiv) was then added dropwise into the bithiophene solution. The colorless reaction turned red immediately upon the addition of n-BuLi, and the reaction mixture was stirred for 2 hr under constant argon flow. The temperature was then allowed to rise to -40 °C and anhydrous DMF (1.75 g, 24 mmol, 8 equiv) was slowly added into the reaction mixture. The reaction was left for stirring overnight, and the temperature was allowed to rise to rt. The cloudy reaction mixture was quenched with an excess of NH_4Cl solution (2M) and was extracted with DCM three times. The combined organic layer was washed with saturated brine, dried over Na_2SO_4 and evaporated under reduced pressure. The yellow crude residue was purified by column chromatography (SiO_2, hexanes-DCM, gradient) to give 1.1 (350 mg, 1.57 mmol, 52.5%) as a golden solid. ^{1}H NMR (400 MHz, $CDCl_3$) δ 9.90 (s, 2H), 7.70 (d, J = 3.9 Hz, 2H), 7.41 (d, J = 3.9 Hz, 2H).

1.2 N,N'-(2,3-dimethylbutane-2,3-diyl)bis(hydroxylamine)

This molecule was synthesized following a method provided by Rajca et al.[40] Aluminum foil (918 mg, 34.1 mmol, 6 equiv) was torn into small pieces roughly sized

0.5 cm×0.5 cm and was put into a 200 mL volume RBF. 3 wt% aqueous $HgCl_2$ solution (548 mg, 2.00 mmol, 0.35 equiv) was then added into the RBF, which was left stirring for about 3-4 minutes at rt. A glass rod was used to mix all aluminum pieces with the cloudy gray solution. Aluminum pieces were soon tarnished. The solution was removed with a pipette, and the amalgamated aluminum pieces were washed with water, methanol, and THF two times each. Note that the washing processes were done quickly because slow washing has once caused fierce bubbling, smoking and heat release. The RBF was then moved to a salt solution ice bath (-10 °C) and 23 mL THF, 3.5 mL water, and a 20 mL THF solution of 2,3-dimethyl-2,3-nitrobutane (1.00 g, 5.68 mmol, 1 equiv) were successively added. The reaction was kept in the salt ice bath and was stirred for 45 minutes to an hour, until no distinct aluminum pieces existed. The reaction mixture was filtered through a narrow pad of celite and washed with THF until no detectable products coming out (a method to indicate the presence of 1.2 can be found in the reference section of an article by Hirel et al.[41]). The filtrate was concentrated under reduced pressure. The residual solid was washed with ether (3×5 mL) to give 1.2 (600 mg, 4.05 mmol, 71.3%) as a white solid. ^{1}H NMR (400 MHz, DMSO-d6) δ 6.93 (s, 2H, OH), 5.35 (s, 2H, NH), 0.95 (s, 12H). IR lit.[42] (powder, ν/cm^{-}1): 3257 (vs. and broad, νOH), 2987 (vs., νC-H), 1479-1374 (vs., several bands), 1261 (s), 1178 (vs.), 1145 (vs.), 1080 (s), 1035 (vs.), 989 (m), 952 (vs.), 904 (vs.), 852 (m), 790 (m), 690 (m).

1.3 2,2'-([2,2'-bithiophene]-5,5'-diyl)bis(4,4,5,5-tetramethylimidazolidine-1,3-diol)

The synthesis of this molecule followed Borozdina's method.[42] 1.1 (150 mg, 675 μmol, 1 equiv) was dried with vacuum and argon flow for three times and then added into 6.75 mL toluene in an oven-dried RBF. A solution of 1.2 (220 mg, 1.48 mmol,

2.2 equiv) in 6.75 mL methanol was mixed with the slurry. The temperature was increased slowly until a clear solution was achieved, usually at around 65 75 °C. The reaction mixture was then left for stirring overnight. Pale yellow precipitates started to form after three hours. A new spot on TLC with Rf=0 (DCM) and the lack of starting material 1.1 spot indicated the completion of the reaction. The solution was allowed to cool to rt and then filtered. The residue was washed with toluene and heptane three times each, dried under high vacuum and a pale yellow solid 1.3 (280 mg, 580 μmol, 86.0%) was achieved. All obtained solids were taken to the oxidation reaction without further purification. ^{1}H NMR (400 MHz, DMSO-d6) δ 7.74 (s, 4H, OH), 6.79 (d, J = 3.6 Hz, 2H), 6.72 (d, J = 3.6 Hz, 2H), 4.46 (s, 2H), 0.79 (s, 24H).

1.4 [2,2'-Bithiophene]-5,5'-bis(nitronyl nitroxide) (informal name)

The synthesis of this molecule followed Borozdina's method.[42] 1.3 (100 mg, 207 μmol, 1 equiv) was added into 5.18 mL of water and 5.18 mL of DCM and was cooled to 0 °C. 5 wt% $NaIO_4$ aqueous solution (674 mmL, 166 μmol, 0.8 equiv) was added dropwise to the slurry. The reaction mixture was left for stirring overnight at rt. The reaction mixture turned dark green after two hours. The disappearance of the reactant 1.3 spot on TLC indicated the completion of the reaction. The reaction mixture was extracted with 3 mL DCM three times, and the organic phase was washed with brine and water. Column chromatography (SiO_2, DCM-Methanol, gradient) was used to purify the compound and gave 1.4 (50.1 mg, 207 μmol, 51%) as dark green solids. The absence of any signal on NMR indicated the presence of unpaired electrons, whose magnetic fields shielded the nuclear spin signals. The structure of 1.4 is further confirmed with MS, X-ray crystallography, and EPR. Mass Spec NMR figure Appendix ESI-MS 476.1544 $[M]^+$: calculated for $[M]^+$ 476.1552

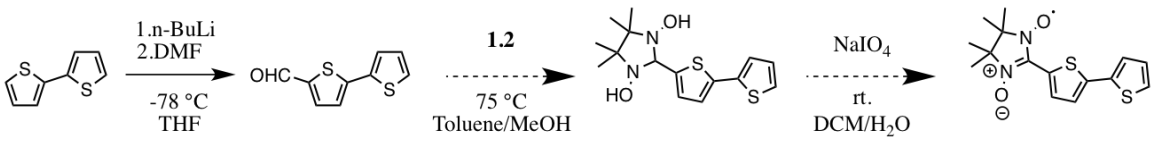

2.1 2.2 2.3

Scheme 1.2: Synthesis of 2.3

Synthesizing 2.3

2.1 [2,2'-bithiophene]-5-carbaldehyde

2.1 is an asymmetric version of 1.1. 2,2 -bithiophene (1.00 g, 6.01 mmol, 1 equiv) was dissolved in 18 mL of anhydrous THF in an oven-dried RBF. The solution was left under argon and cooled to -78 °C. A 2.5M hexanes solution of n-BuLi (2.41 mL, 6.01 mmol, 1 equiv) was then added dropwise into the bithiophene solution. The colorless reaction turned dark orange immediately upon the addition of n-BuLi, and the reaction mixture was stirred for 2 hr under constant argon flow. The temperature was then allowed to rise to -40 °C and anhydrous DMF (1.76 g, 24.06 mmol, 4 equiv) was slowly added into the reaction mixture. The reaction was left for stirring overnight, and the temperature was allowed to rise to rt. The cloudy reaction mixture was quenched with an excess of NH_4Cl solution (2M) and was extracted with DCM three times. The combined organic layers were washed with DI water, dried over Na_2SO_4 and evaporated under reduced pressure. The red crude residue was then dissolved in small amount of DCM and purified by column chromatography (SiO_2, hexanes-DCM, gradient) to give 2.1 (330 mg, 1.70 mmol, 28.2 %) as a yellow solid. A trace amount of impurity would result in brownish or purple color. ^{1}H NMR (400 MHz, DMSO-*d*6) δ 9.85 (s, 1H), 7.965 (d, J = 4.0 Hz, 1H), 7.68 (d, J = 5.0, 1.2 Hz, 1H), 7.565 (d, J = 3.7, 1.2 Hz, 1H), 7.495 (d, J = 4.0, 1 Hz, 1H), 7.14(t, J = 5.1, 3.7 Hz, 1H).

2.2 2-([2,2'-bithiophen]-5-yl)-4,4,5,5-tetramethylimidazolidine-1,3-

diol 2.1 (30 mg, 154,43 μmol, 1 equiv) was dried with vacuum and argon flow for three times and then added into 0.2 mL toluene in an oven-dried RBF. A solution of 1.2 (25.18 mg, 169.87 mmol, 1.1 equiv) in 0.2 mL methanol was mixed with the slurry. A clear solution was achieved without increasing temperature. The reaction mixture was then left for stirring overnight. No precipitation formed while a new polar spot appeared on the baseline of TLC. The solution was allowed to cool to rt and solvent evaporated. Clean products were not obtained.

2.3 [2,2'-Bithiophene]-5-nitronyl nitroxide 2.2 (50 mg, 154.10 μmol, 1 equiv) was added into 1.54 mL of water and 1.54 mL of DCM, and was cooled to 0 °C. 5 wt% $NaIO_4$ aqueous solution (0.501 mmL, 123.28 μmol, 0.8 equiv) was added dropwise to the slurry. The reaction mixture was left for stirring overnight at rt. The reaction mixture turned dark purple after two hours. A purple spot on TLC (DCM as solvent) with RfH=0.4 appeared. The reaction mixture was extracted with 3 mL DCM three times, and the organic phase was washed with brine and water. Column chromatography (SiO_2, DCM-Methanol, gradient) compound and the purple spot on TLC was isolated. However, MS and UV-Vis spectrum indicated the product did not possess desired structure. The synthesis of 2.2 and 2.3 was repeated three times with varied conditions, but all gave the same incorrect product. ESI-MS 306.09 [M^+] The mass spec indicates the sample being a thiophene-2-iminyl nitroxide.

Synthesizing 3.6

3.1 3,3'-dihexyl-2,2'-bithiophene

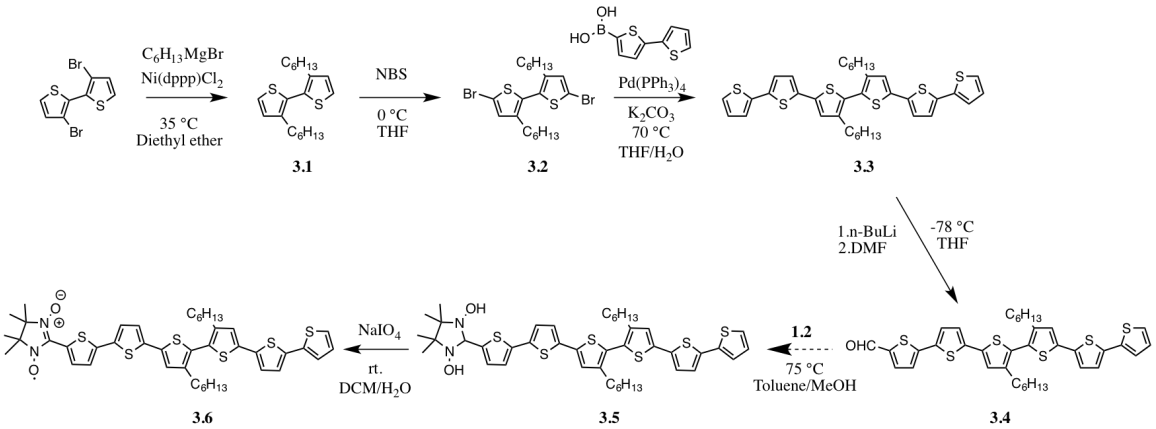

Scheme 1.3: Synthesis of 3.6

3.2 5,5'-dibromo-3,3'-dihexyl-2,2'-bithiophene

The synthesis of 3.1 and 3.2 followed procedures provided by Bhuwalka et al.[43]

3.3 3"',4"-dihexyl-2,2':5',2":5",2"':5"',2"":5"",2"""-sexithiophene

A mixture of 3.2 (428 mg, 0.870 mmol), [2,2'-bithiophen]-5-ylboronic acid (402 mg, 1.91 mmol) and $Pd(PPh_3)_4$ (101 mg, 0.087 mmol) was degassed and backfilled with argon three times before 13 mL THF and 3 mL 2M K_2CO_3 aqueous solution were added by syringe. The reaction mixture was stirred at 70 °C overnight before washed with saturated aqueous NH_4Cl solution and extracted with DCM. The organic layer was dried over anhydrous Na_2SO_4 and purified by column chromatography (SiO_2, 1:20 EtOAc-hexanes) to give the product as a yellow solid (300 mg, 52%). ^{1}H-NMR (400 MHz, $CDCl_3$): δ = 7.21 (dd, J = 5.1, 1.1 Hz, 2H), 7.16 (dd, J = 3.6, 1.2 Hz, 2H), 7.07 (d, J = 3.8 Hz, 2H), 7.05 (d, J = 3.8 Hz, 1H), 7.03 (s, 1H), 7.01 (dd, J = 5.1, 3.6 Hz, 2H), 2.51 (t, J = 7.0 Hz, 4H), 1.57 (p, J = 7.0 Hz, 4H), 1.25 (m, 12H), 0.85 (t, J = 7.0 Hz, 6H).

3.4 3"',4"-dihexyl-[2,2':5',2":5",2"':5"',2"":5"",2"""-sexithiophene]-

5-carbaldehyde

3.3 (100 mg, 150.82 μmol, 1 equiv) was dissolved in 1.5 mL of anhydrous THF in an oven-dried RBF. The solution was left under argon and cooled to -78 °C. A 2.5M hexanes solution of n-BuLi (722 mmL, 150.82 μmol, 1 equiv) was then added dropwise into the bithiophene solution. The colorless reaction turned red immediately upon the addition of n-BuLi, and the reaction mixture was stirred for 2 hr under constant argon flow. The temperature was then allowed to rise to -40 °C and anhydrous DMF (22.05 mg, 301.63 μmol, 2 equiv) was slowly added into the reaction mixture. The reaction was left for stirring overnight and the temperature was allowed to rise to rt. The cloudy reaction mixture was quenched with an excess of aqueous NH_4Cl solution (2M) and was extracted with DCM three times. The combined organic layers were washed with DI water, dried over Na_2SO_4 and evaporated under reduced pressure. The orange crude residue was then dissolved in small amount of DCM and purified by column chromatography (SiO_2, hexanes-DCM, gradient) to give 3.4 (14 mg, 20.26 μmol, 13.4%) as a red solid. 1H-NMR (400 MHz, CDCl3): δ = = 9.85 (s, 1H), 7.66 (d, J = 4.0 Hz, 1H), 7.26 (d, J = 3.8 Hz, 1H), 7.24 – 7.20 (m, 2H), 7.17 (dd, J = 3.6, 1.2 Hz, 1H), 7.10 (d, J = 3.9 Hz, 1H), 7.09 (s, 1H), 7.07 (d, J = 3.8 Hz, 1H), 7.05 (d, J = 3.8 Hz, 1H), 7.04 (s, 1H), 7.01 (dd, J = 5.1, 3.6 Hz, 1H), 2.48-2.55 (m, 4H), 1.22-1.29 (m, 16H), 0.82-0.87 (m, 6H).

3.5 2-(3”’,4”-dihexyl-[2,2’:5’,2”:5”,2”’:5”’,2””:5””,2”””-sexithiophen]-5-yl)-4,4,5,5-tetramethylimidazolidine-1,3-diol

3.4 (14.0 mg, 20.3 μmol, 1 equiv) was dried with vacuum and argon flow for three times and then added into 0.1 mL toluene in an oven-dried RBF. A solution of 1.2 (4.50 mg, 20.26 μmol, 1.5 equiv) in 0.1 mL methanol was mixed with the slurry. The temperature was increased slowly until a clear solution was achieved, usually

at around 65 75 °C. The reaction mixture was then left for stirring overnight. No precipitation formed during reaction. A new spot on TLC with Rf=0 (DCM) and the absence of the starting material 3.4 spot indicated the completion of the reaction. The solution was dried with rotary evaporator. Clean products were not obtained. All solids (17 mg) were taken to the oxidation reaction without further purification.

3.6 Sexithiophene mono-Nitronyl-Nitroxide radical

Crude 3.5 (17 mg, 20.7 μmol, 1 equiv) was added into 0.1 mL of water and 0.1 mL of DCM and was cooled to 0 °C. 5 wt% $NaIO_4$ aqueous solution (33.66 mmL, 8.28 μmol, 0.4 equiv) was added dropwise to the slurry. The reaction mixture was left for stirring overnight at rt. The reaction mixture turned dark green after two hours. The disappearance of the starting material 3.5 Rf=0, spot on TLC indicated the completion of the reaction. The reaction mixture was extracted with 0.1 mL DCM three times, and the combined organic layers were washed with brine and water. Column chromatography (SiO_2, DCM-methanol, gradient) was used to purify the compound and gave 3.6 (3 mg, 3.67 μmol, 17.7%) as black solids. The absence of any signal on NMR indicated the presence of unpaired electrons, whose magnetic fields shielded the nuclear spin signals. ESI-MS 817.21 [M^+], Calculated for 817.21 [M^+]

1.3 Results and Discussion

1.3.1 Synthesis

1.2

2,3-Bis(hydroxyamino)-2,3-dimethylbutane (1.2) is the key reagent in the synthesis of nitronyl nitroxide derivatives. Traditionally, 1.2 was made according to Ullman's

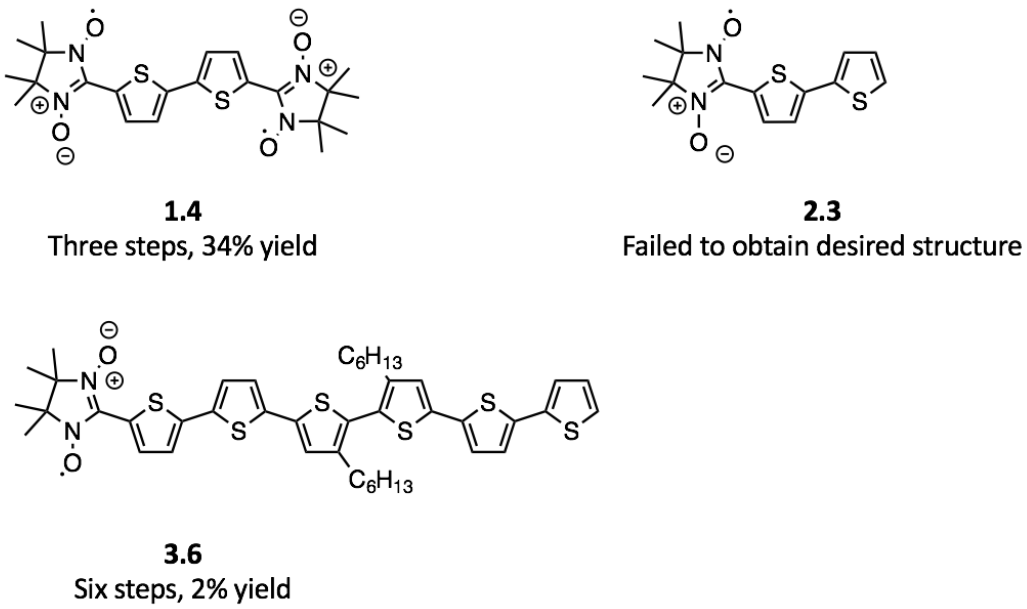

Figure 1.4: Products yield

procedure,[41,44] where zinc was used as the reducing agent and NH_4Cl as the ligand. However, Ullman's procedure failed to give desired products. Several modifications have been made, including using zinc power of smaller sizes, changing the order of adding reagents, increasing reaction time and altering the solvent ratio, but none of them were effective. Hirel et al. mentioned that the blue color, which indicated the presence of nitroso intermediate disappeared upon the completion of the reaction, but such process was never observed.[41] The isolated products in the Egap lab were always identified as dinitrobutane, which was the starting material, and acetone oxime, a decomposed product of hydroxylamine. Several factors may have caused the failure in synthesis. First, all works of literature synthesized 1.2 in large scale (17.6 g starting material) in a reactor with mechanical stirring, while the Egap lab lacked such reactor and so 1.2 was synthesized in one-gram scale with much weaker stirring by a magnetic stir bar. Second, l extracted 1.2 with Soxlet apparatus, which was inefficient in small scale experiments. Third, the reduction potential (-0.76 E^0) of zinc is too low.

Instead, an alternative method using Al/$HgCl_2$ amalgam as the reducing agent was taken to reduce the dinitro compound, and a 71.3% yield, which was better than the yield of Ullman's procedure, of pure 1.2 was achieved.[41] Nonetheless, this method was only suitable for small-scale (¡1 g starting material) reactions because of the toxicity of mercury compounds. Also, the amalgam could be extremely reactive if placed near a heat source, such as a vacuum pump. During two attempts to synthesize 1.2, intensive bubbling and heating were observed during the washing process, and gray smoke filled the round bottom flask; both attempts resulted in a very low yield of product. Therefore, this reaction is recommended to be proceeded under low temperature, preferably 0 °C, although doing so may reduce the overall yield.

The synthesis of 1.4 started from deprotonation of bithiophene with excess n-butyl lithium and followed by quenching with excess anhydrous DMF (Scheme 1.1). 1.1 was obtained in 79% yield after purification by column chromatography. Condensation of 1.1 and three equivalents of 1.2 in toluene at 75 °C generated 1.3 in 85% yield. 1.3 precipitated due to the low solubility of four hydroxyl groups as the reaction proceeded. Filtered pale yellow solids were washed with toluene and heptane. NMR spectrum indicated the rather high purity of 1.3 with a slight presence of partially reacted compound. 1.4 was obtained in 50% yield by oxidation of 1.3 with aqueous sodium periodate solution and was purified by column chromatography. The overall yield of 1.4 was 34% in three steps.(Figure 1.4)

The attempts to synthesize 2.3 started from 2.1, which was obtained by one-side deprotonation of bithiophene with one equivalence of n-butyl lithium, followed by quenching with excess anhydrous DMF(Scheme 1.2). After extraction, washing, and concentration, 2.1 as brownish-red crude solids were obtained. TLC (SiO_2, DCM) indicated the presence of two red impurities, both of which ran faster than the product spot on TLC. Pure 2.1 (23% yield), indicated by TLC, was achieved after column chromatography, but the same red impurities reappeared after concentration under

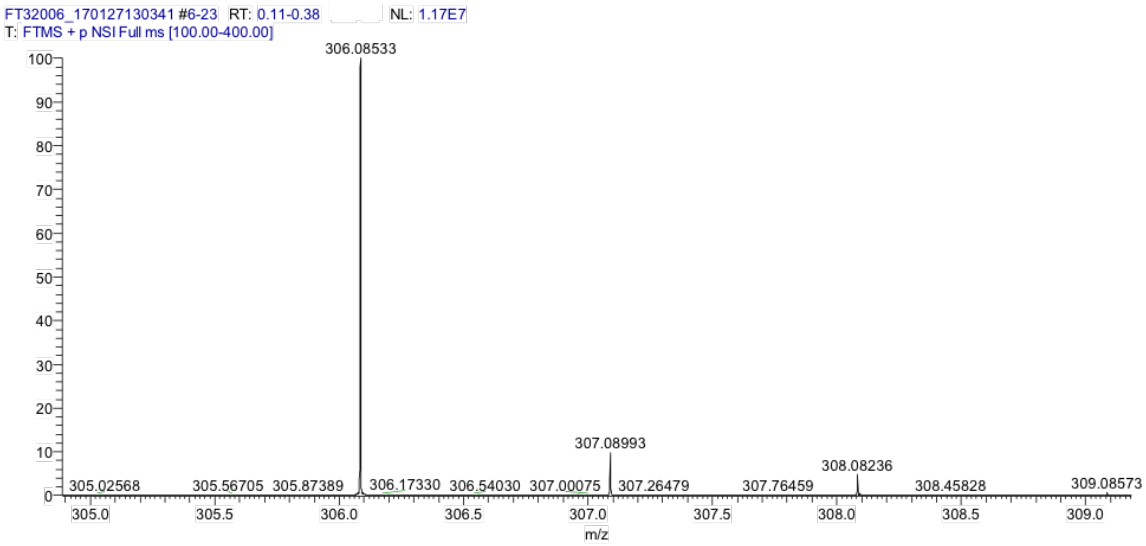

Figure 1.5: ESI-MS of the product from the synthesis of 2.3

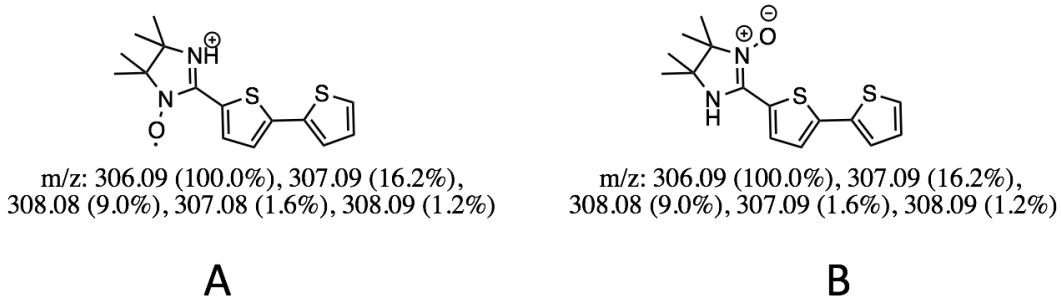

Figure 1.6: ESI-MS results and computed m/z indicate the product from the synthesis of 2.3 is either A or B or a mixture

rotatory evaporator. However, the NMR spectrum of 2.1 displayed significant purity. Hence, this batch of 2.1 was taken to the next step without further purification. Due to the fewer hydroxyl groups present in 2.2, it was much more soluble than 1.3, and 2.2 did not precipitate even though reaction concentration was raised five times higher. Purification of 2.2 was not achievable, and NMR of the crude compound was messy, as expected. All crude 2.2 was taken to the oxidation step. ESI-MS(Figure 1.5) indicated that the resulting products of the attempted synthesis were either compound A or B.(Figure 1.6)The same products were generated after several modifications, such as

adding less oxidant, lowering reaction temperature and changing solvent ratio. After one and half month's attempts and obtaining same structures, the synthesis of 2.3 was abandoned. Some impurities from the first and second step could have resulted in the undesired products.

To study the property of thiophene mono-radical and make comparison with di-radical systems, 3.6 was synthesized and analyzed because sexithiophene-bis(nitronyl nitroxide) (T6DR, Figure 1.3) has been synthesized in the Egap lab previously. Hexyl chains were installed onto the two central thiophene rings to increase the solubility of the sexithiophene-mono radical, which would otherwise be insoluble due to strong π-stacking forces. Alkylated sexithiophene derivative, 3.3, was made from conjugating [2,2'-bithiophene]-5-ylboronic acid and dibrominated compound, 3.2, through Suzuki coupling and the yield was 52%. One-side deprotonation with n-butyl lithium followed by quenching with DMF gave 13.4% yield of 3.4, which was purified by column chromatography. Due to the high solubility of 3.5, it did not precipitate when the condensation reaction ended. Solvent was evaporated, and all solids were taken to the oxidation step without further purification. The oxidation reaction followed by column chromatography gave 17.7% yield of 3.6, whose structure was confirmed with ESI-MS and the 700 nm absorbance, a distinctive feature of the radical, on the UV-Vis spectrum. (Scheme 1.3)

1.3.2 Crystal Structure of 1.4

X-ray crystallography gave structural information of 1.4 asymmetric unit and crystal packing pattern.(TableA.1) An asymmetric unit of 1.4 contains two molecules with similar geometry, and four asymmetric units form one triclinic crystallographic unit cell, with a P-1 space group.(Figure 1.7) Both molecules in the asymmetric unit are planar, indicated by small torsion angles, the largest torsion being less than 10° between two central thiophene rings, as well as between one thiophene ring and one

imidazoline ring. The planar structure is further stabilized by short intramolecular distance, 2.753 Å between S1···O2 and S2···O3. The overall conjugated coplanar structure facilitates spin polarization as well as charge transfer between the radicals and bithiophene coupler, as interpreted by Tretyakov et al. in their study of a similar compound.[45]

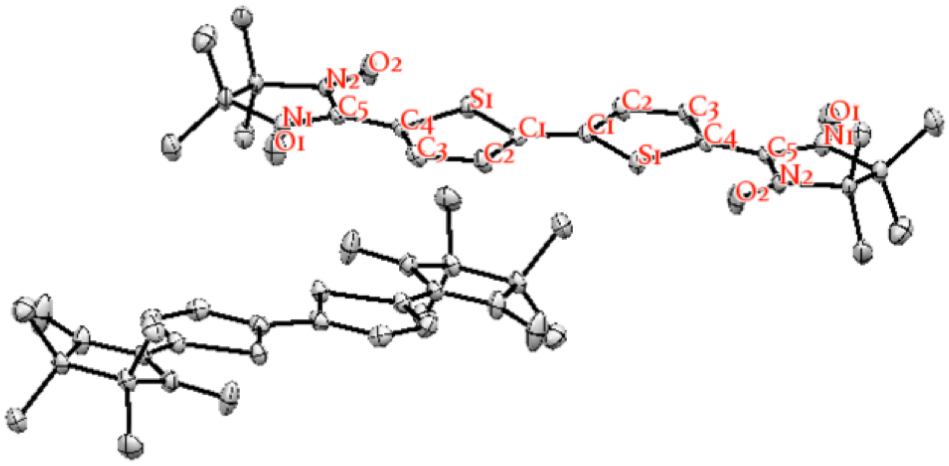

Figure 1.7: The asymmetric unit of 1.4 contains two planar molecules. The coplanar structure can facilitate spin polarization as well as charge transfer.

Parallel displaced π-stacking along the 0-11 direction with an intermolecular distance of 3.498 Å is the driving force of crystal formation. (Figure 1.8) π-stacking has also been the driving force for the formation of T6DR crystals. The prevalence of π-stacking in the crystals of thiophene-radical pairs shows that the addition of NN radicals extended the conjugated π system and did not have other unexpected impacts on crystal morphology. A single crystal of 3.6 was not obtained and thus not studied.

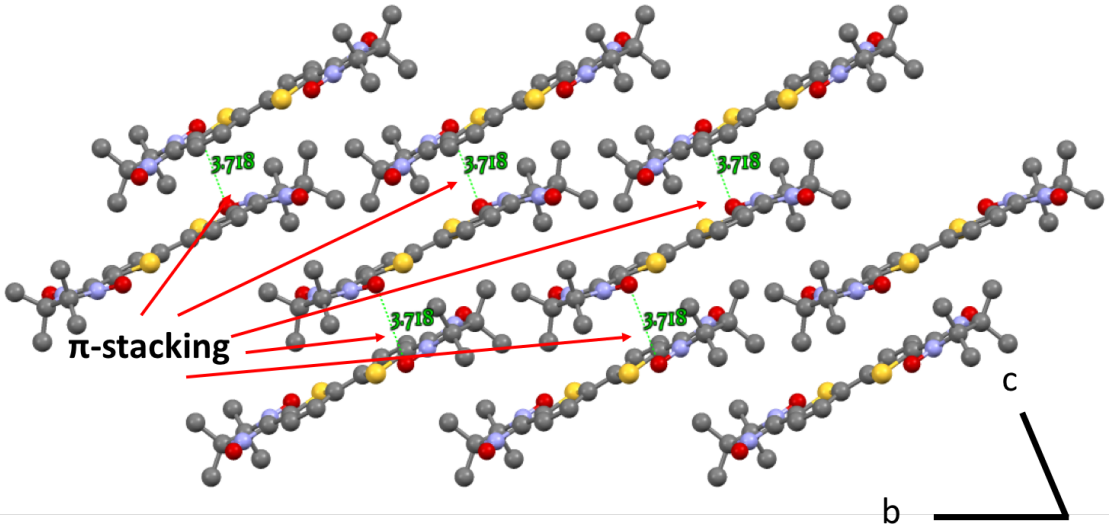

Figure 1.8: The parallel-displaced π-stacking along the 0-11 direction with an intermolecular distance of 3.498 Å is the driving force of crystal formation

1.3.3 EPR Spectra of 1.4

The EPR spectra of 1.4 taken under 20, 30 and 40 dB microwave power are shown in figure 1.9. Spectra were obtained under different acquisition conditions to optimize the acquisition parameters and to reveal impurities. The uniformity of the spectra shows the purity of the sample. The biradical spectrum centered at 336.0 mT shows significant resolution of features, suggesting an intramolecular electron-electron interaction, which is consistent with the proposed structure and biradical nature of 1.4.

A common feature of biradicals is a "half-field transition" (HFT) that occurs at approximately one-half of the magnetic field value of the primary EPR spectrum in the g 2 region. The HFT is a "forbidden transition," and has an amplitude about 10^3-10^4 -fold lower than the primary transitions, which makes its observation very difficult at high noise level. HFT of 1.4 was observed at 168.0 mT, under a relatively high microwave power of 20 dB and the help of 10-fold higher field modulation amplitude. The clarity of the HFT signal signifies the homogeneity of the sample. (Figure 1.10)

Temperature controlled EPR experiments are needed to understand the radical

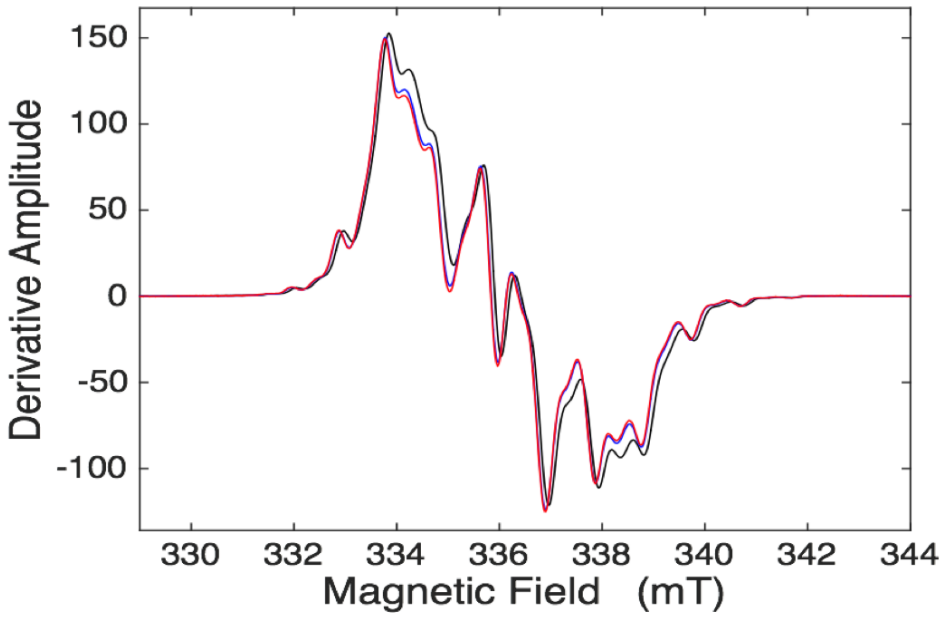

Figure 1.9: The EPR spectra of 1.4 under 20 (black), 30 (blue), 40 (red) dB microwave power

spin alignment, either ferromagnetic or antiferromagnetic, at the ground state. Mitsumori et al. have explained that due to the weak magnetic susceptibility of IN, another type of radical that has similar structure as NN, the two radical components linked to chromophore have almost no magnetic interactions, which means ferromagnetic and antiferromagnetic alignment of radicals at ground state do not have much energy difference. The OTNN ground state spin alignment is still not experimentally measured. However, computational approaches have shown that antiferromagnetic and ferromagnetic alignment both exist in ground state and are degenerate. This will be presented in the computation section.

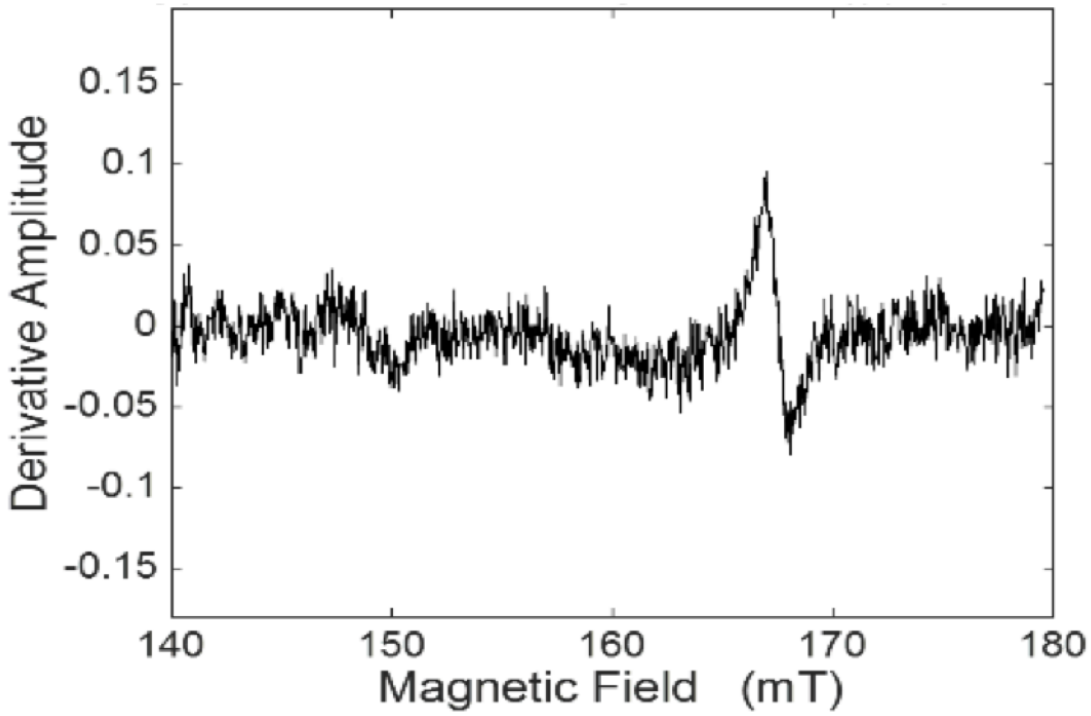

Figure 1.10: Clear HFT signals in the EPR spectra of 1.4 suggest high purity of the sample

1.3.4 Steady-State Absorption

OT2 and 1.4

The steady-state UV-vis spectra of 1.4 and bithiophene in toluene are shown in figure 1.11. The major peak has a λ_{max} at 402 nm, with a molar absorptivity of 3.83×10^4 $M^{-1}cm^{-1}$,originates from the π-π^* transition of bithiophene and nitronyl nitroxide.[33,44](Table 1.1) As shown in figure1.11, the absorption peak of π-π^* transition red-shifts for 97 nm because of the strong electronic coupling between the radicals and the chromophore. A minor and broad absorption was observed at peak maximum of 686 nm, with a molar absorptivity of $8.42\times10^2M^{-1}cm^{-1}$, about 45 fold weaker than the primary 402 nm absorption. This minor absorption is supposedly from a n-π^* transition that has a charge-transfer character because an absorption peak of similar pattern and wavelength on PhNN monoradical.[44] The n-π^* nature of

Table 1.1: Steady-state optical properties of OT2,1.4,OT6,3.6 and T6DR

cpd	$\lambda_{\pi\text{-}\pi^*}$ (nm)	$\lambda_{n\text{-}\pi^*}$ (nm)	λ_{em} (nm)	ϕ_F
OT2	305	-	368	3.2%
OT6	390	-	512, 539	43%
1.4	402	686	-	0
3.6	414	702	517	2.5%
T6DR	425	707	-	0

the transition near 600 nm in PhNN absorption spectrum is explained by the Ullman group and confirmed through the observation of blue-shifted spectrum at increased solvent polarity. The PhNN absorption shifted from 625 nm in toluene to 586 nm in acetonitrile.(Figure1.12) The dependence of absorption wavelength on solvent polarity is a trait of charge-transfer (n-π^*) character.[44] The molecule at ground-state has lower energy in polar solvents, which is MeCN in this case, so the excitation energy needed is higher. Since 1.4 was insoluble in MeCN, T6DR(Figure 1.3), which has a longer thiophene conjugation length but similar symmetry as 1.4, was used to perform the experiment. The absorption wavelength dependence on solvent polarity was not observed in T6DR.(Figure 1.12) This is because the n-π^* transition takes place at both ends, i.e. the two radical components of the T6DR molecules. The induced dipole-change on both ends cancel the effect of one another, and thus the net change in the polarity of the molecule is minimal. Without altered polarity upon n-π^* transition, the solvent dependence of absorption wavelength will be much weaker. The n-π^* transition in PhNN has much stronger solvent dependence because the molecule is

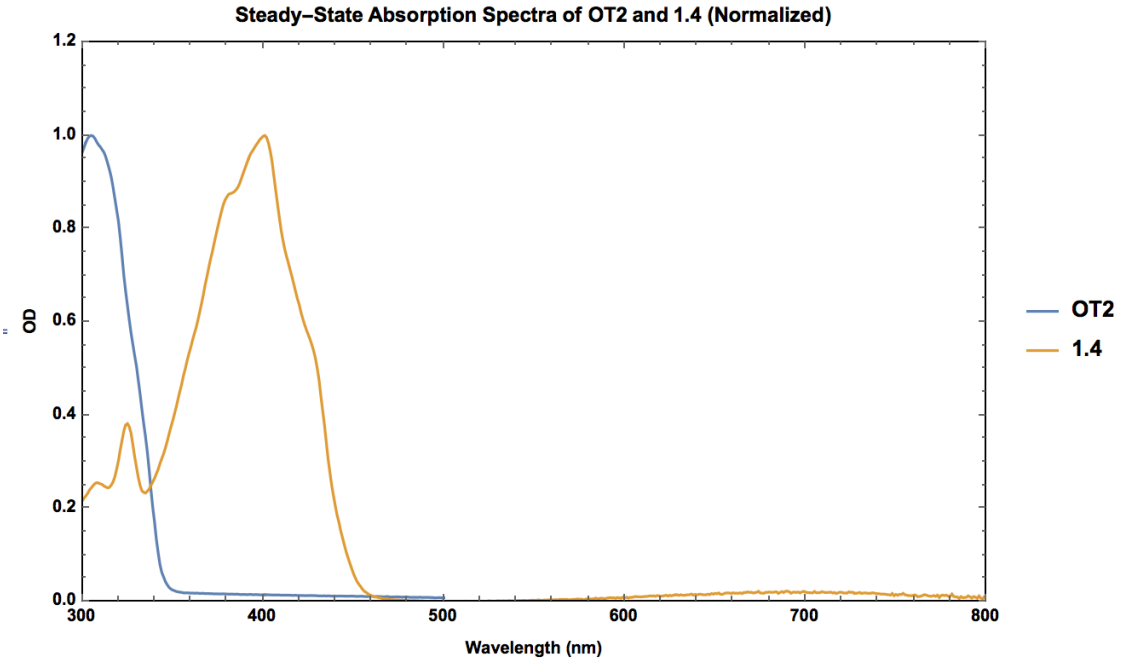

Figure 1.11: The steady-state absorption spectra of OT2 and 1.4. Strong electronic coupling between oligothiophene and nitronyl nitroxide components result in the 97 nm red-shift at λ_{max} of π-π^* transition.

asymmetric in terms of dipole change, and thus charge-transfer induced dipole change is large.

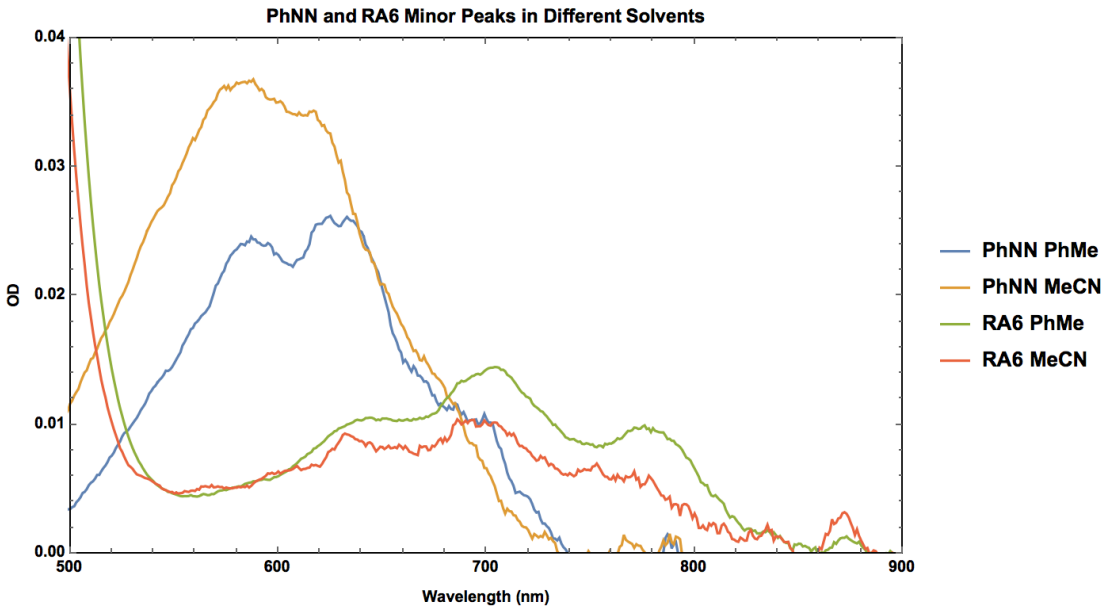

Figure 1.12: The steady-state absorption spectra of n-π^* of PhNN and T6DR in toluene (non-polar) and acetonitrile (polar) are compared. In acetonitrile, the λ_{max} of n-π^* in PhNN blue-shifts. T6DR peaks remain constant regardless of solvent because the dipole change induced by two symmetrical n-π^* transitions cancel.

OT6, 3.6 and T6DR

The steady-state UV-vis absorption of OT6, 3.6 and T6DR are shown in figure. Similar to the spectrum of 1.4, 3.6 has two absorption peaks, with λ_{max} at 414 nm (molar absorptivity=6.17×10^3 $M^{-1}cm^{-1}$) and 702 nm (molar absorptivity = 5.9×10^1 $M^{-1}cm^{-1}$). Compared with the absorption spectrum of T6DR, whose λ_{max} is at 425 nm, the spectrum of 3.6 has less red-shift regarding OT6 λ_{max} at 389 nm. Also, the ratio of the absorption at λ_{max} of the major peak to that of minor peaks near 700 nm is 50 in T6DR and 100 in 3.6. These two phenomena both are caused by the fact that 3.6 has one less radical component than T6DR, which results in a smaller conjugated structure, less electronic coupling, and one-half probability of n-π^* transition.

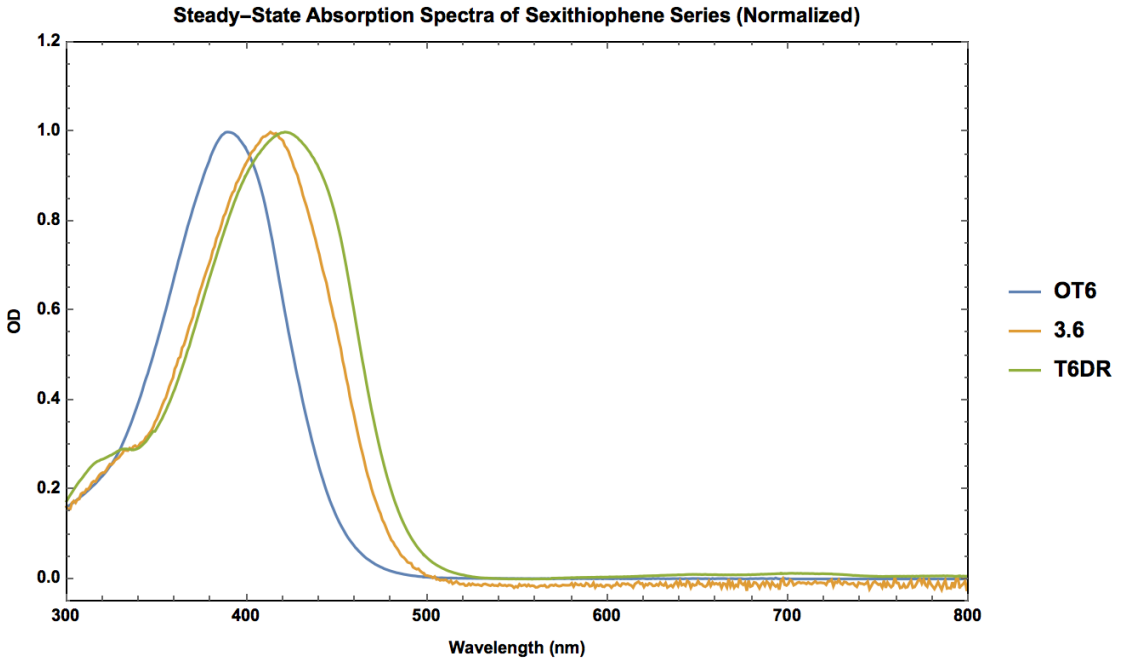

Figure 1.13: The steady-state absorption spectra of OT6, 3.6 and T6DR. Comparing with T6DR, 3.6 has a smaller n-π^* absorption (almost merged with background noise)and less red shift regarding OT6 because 3.6 has one less radical component and a smaller conjugated structure

1.3.5 Steady-State Emission

The Φ_F of OT2, 1.4, OT6, 3.6 and T6DR is computed according to the following equation:[46]

$$\Phi_X = \Phi_{ST} \frac{I_X}{I_{ST}} \frac{\eta_X^2}{\eta_{ST}^2} \frac{A_{ST}}{A_X} \tag{1.1}$$

where X refers to the measured sample, ST refers to the standard (Rho 6G), Φ refers to fluorescence quantum yield, I refers to the integration of fluorescence signals, η refers to refraction index of the solvent used and A refers to the absorption intensity at the excitation wavelength.Φ_F of the standard is 1, and Φ_F of samples are expressed in percentage.

OT2 and 1.4

The maximum of OT2 fluorescence emission is at 368 nm, and the measured Φ_F is 3.2%, in accordance with the literature.[33] Although OT2 already has the lowest fluo-

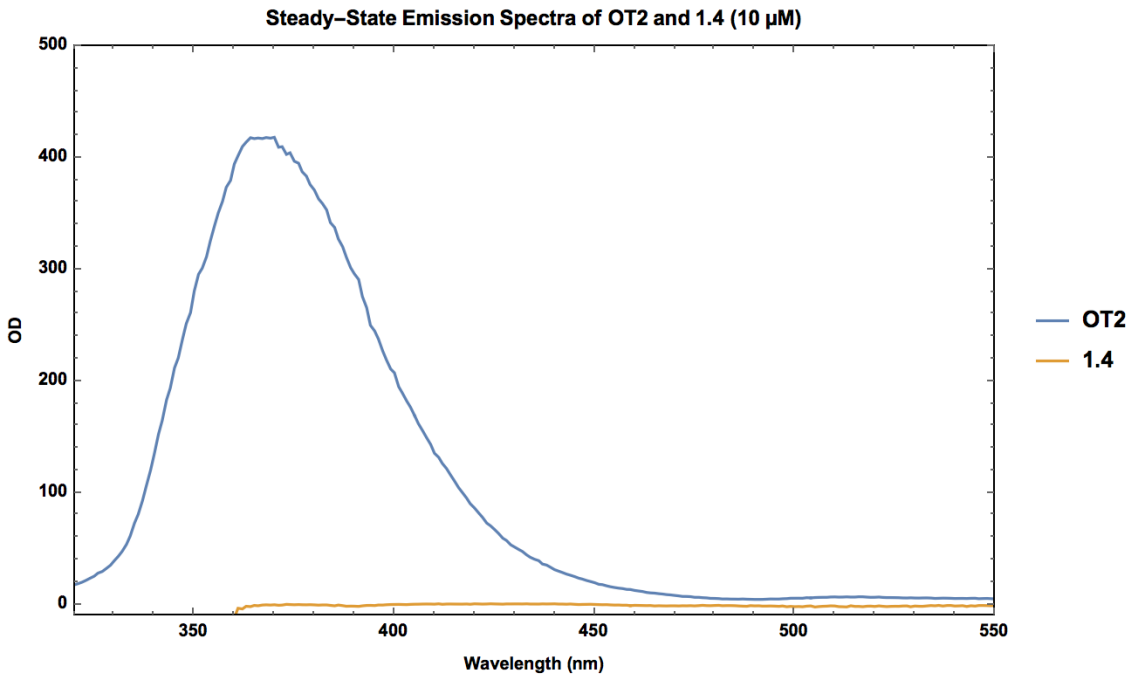

Figure 1.14: The steady-state emission spectra of OT2 and 1.4. The 1.4 signals are completely unidentifiable due to fluorescence quenching

rescence quantum yield among all oligothiophenes, the quantum yield of 1.4 was much less than that of OT2.(Figure 1.14) In fact, the fluorescence signals of 1.4 completely merge with background noise regardless of concentration or excitation/emission slit width. Therefore, the fluorescence quantum yield of 1.4 is considered as 0. Fluorescence quenching, although not ubiquitous, is common among organic radicals with chromophore-radical structure, and is explained by multiple relaxation pathways such as charge transport, EISC, and EIC.[11] The reason for fluorescence quenching in this system will be elaborated in the transient absorption section.

OT6, 3.6 and T6DR

Unlike diradicals 1.4 and T6DR, whose fluorescence signals are unresolvable regardless of measurement conditions, monoradical 3.6 has a clear fluorescence peak at 517 nm and 2.5% quantum yield.(Figure 1.15) This observation shows that the fluorescence quenching depends on not only the presence of radical but also on the number of radicals.

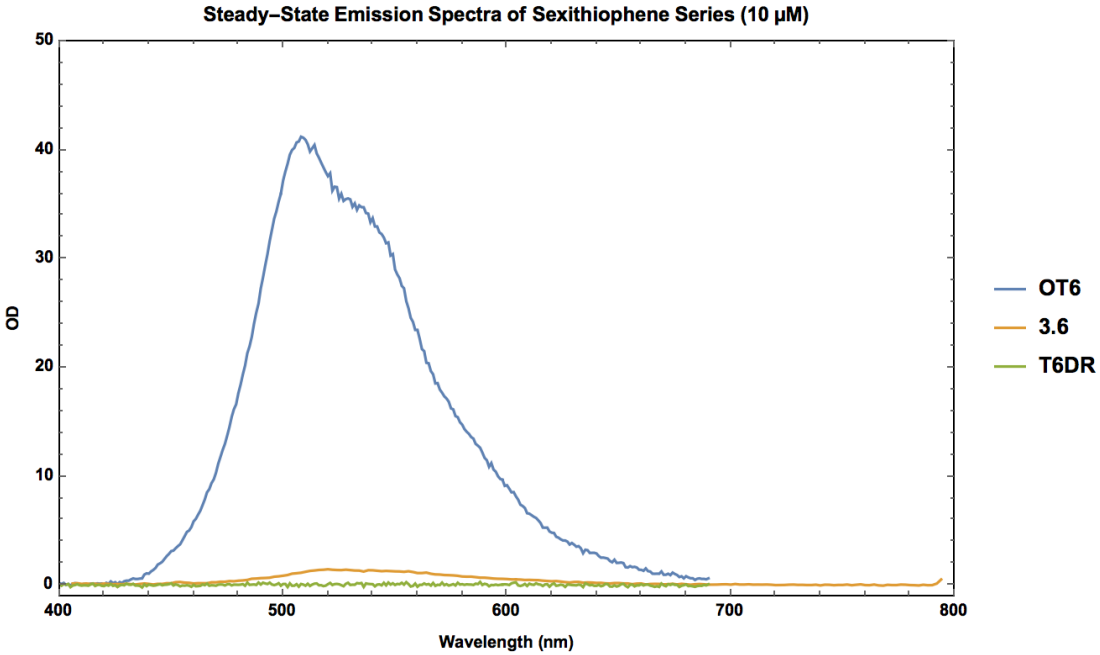

Figure 1.15: The steady-state emission spectra of OT6, 3.6 and T6DR. Unlike the diradicals, 3.6 has identifiable fluorescence signals because 3.6 has one less radical component.

1.3.6 Excited-states Analysis

The transient absorption spectra provide insights into the excited state optical properties of 1.4, 3.6 and T6DR All three samples were excited with a 400 nm laser. The absence of the signal on the spectra near 800 nm was caused by the excitation light residue. T6DR was excited at 650 nm as well to investigate the nature of the weak absorption band near this wavelength. Due to the low solubility of 1.4 in toluene and low absorption intensity, 650 nm excitation of 1.4 was unsuccessful. 3.6 dissolved well in toluene but its molar absorptivity at 650 nm was too weak, so an experiment with 650 nm excitation was not proceeded.

OT2 and 1.4

The first species occurs as a broad peak that centers at 667 nm within system response time of the femtosecond instrument. It decays within 0.20 ps.(Figure 1.16) This is followed by the simultaneous rise of another two broad peaks with $\lambda_{\max}$ at 507 nm and 834 nm, which last for 161 ps.(Figure 1.16) Both are attributed to the second species. The second species is also observed in the nanosecond spectra. Although 1.4 has two transient species like OT2, the nature of the two species in 1.4 and OT2 are significantly different. The first species in OT2 is the singlet excited state (OT2 S_1), which rises within system response time, decays at $k_F = 0.55$ ns^{-1} and has a lifetime of 0.046 ns in benzene.[33] The first transient species of OT2 decays through fluorescence. The second species is OT2's triplet excited state(s) (OT2 T_{1-4}), signified by its triplet-to-triplet absorption $\lambda_{\max}$ (T-T_{max}) at 370 nm. The corresponding intersystem crossing rate is $k_{ISC} = 18.6$ ns^{-1} and the lifetime of the triplet state is 124 μs.[33] None of the shape, decay kinetics or lifetime of the two species in 1.4 resemble those of OT2, which reflects the significantly different electronic structure of 1.4 comparing with OT2.

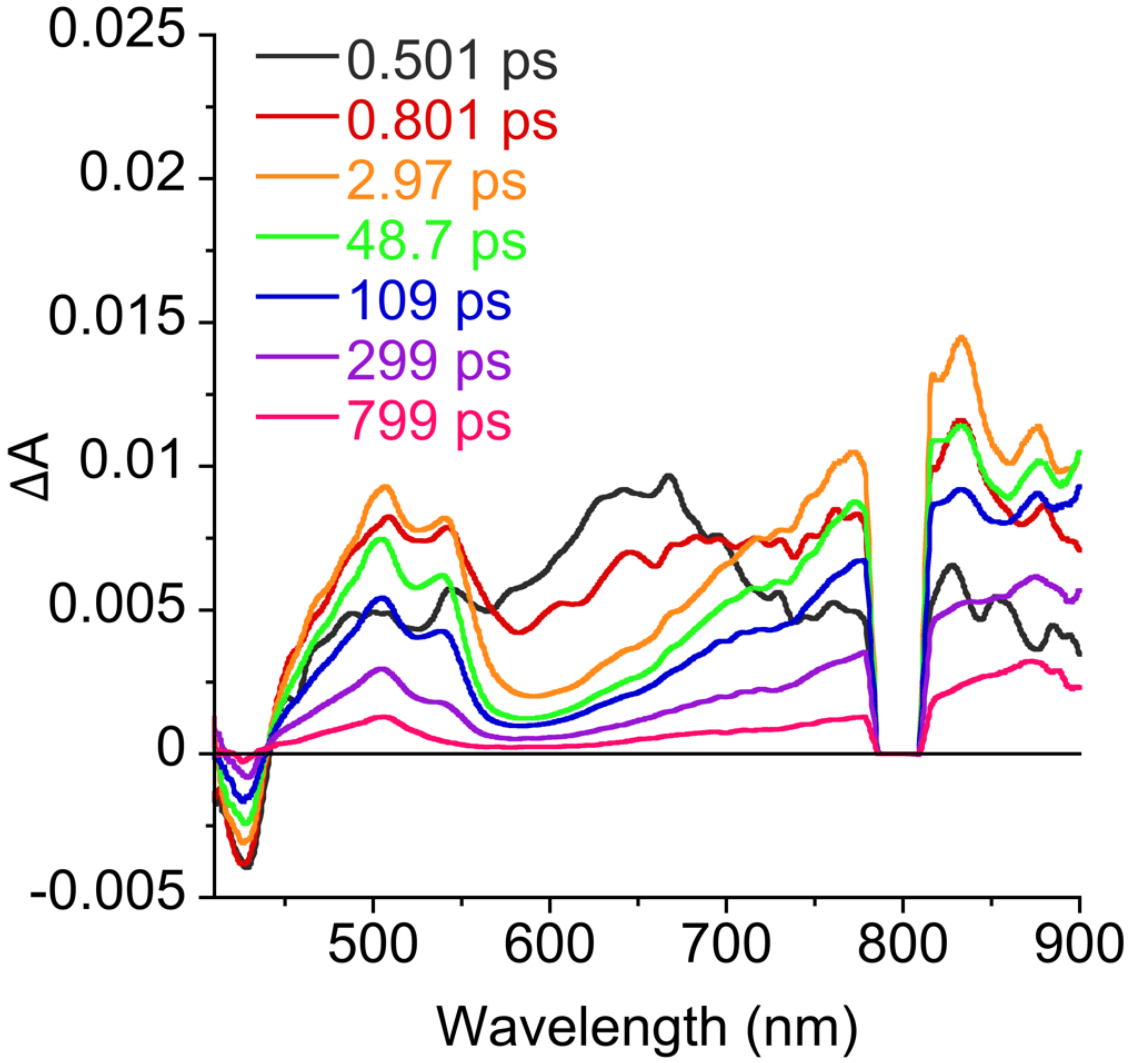

Figure 1.16: Time-resolved excited-state absorption spectra of 1.4. Two species are generated after photoexcitation. The first one has a 667 nm $\lambda_{\max}$ and is attributed to the absorption of S_H states. The second species features 507&834 nm $\lambda_{\max}$ and is attributed to the absorption of S_{CT} states.

OT6, 3.6 and T6DR

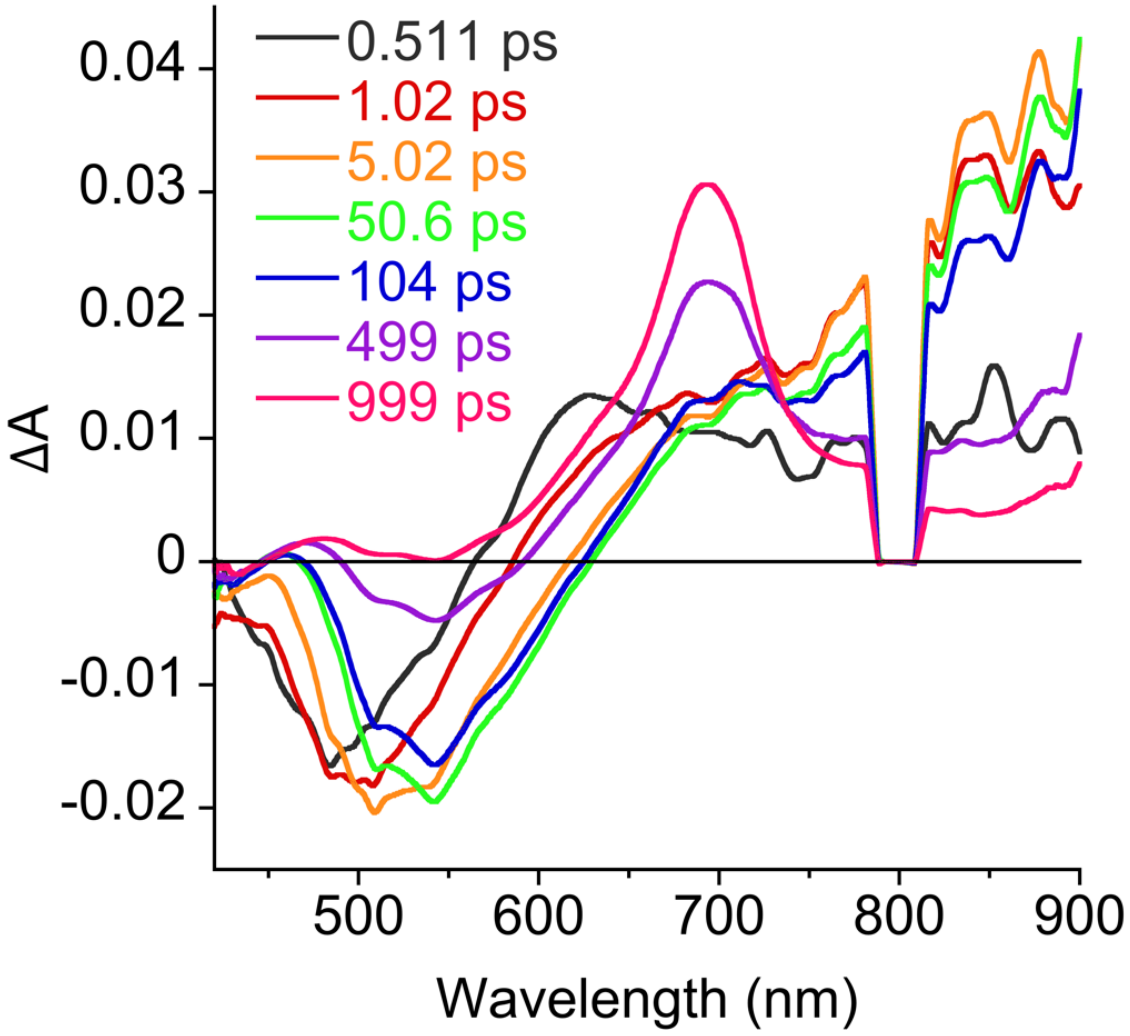

Figure 1.17: Time-resolved excited-state absorption spectra of OT6 (femtosecond laser). The first transient species in OT6 is S_1 featuring emission at 500-600 nm and absorption near 660 nm and 900 nm. The second transient species is attributed to T_1 and has 710 nm $\lambda_{\max}$, which is the T-T_{max} absorption. Neither of these two states exist in OTNN systems.

Although OT6 has two hexyl chains, which distort the conjugated structure, its electronic structure is similar to unsubstituted sexithiophene.[33] OT6 has 44% Φ_F and the fluorescence lifetime is 0.32 ns.(Table 1.1) Its triplet has a T-T_{max} absorption of 710 nm and the lifetime is in the microsecond range.(Figure 1.18) Neither of the two features of OT6 remains in T6DR. The two species in the transient absorption

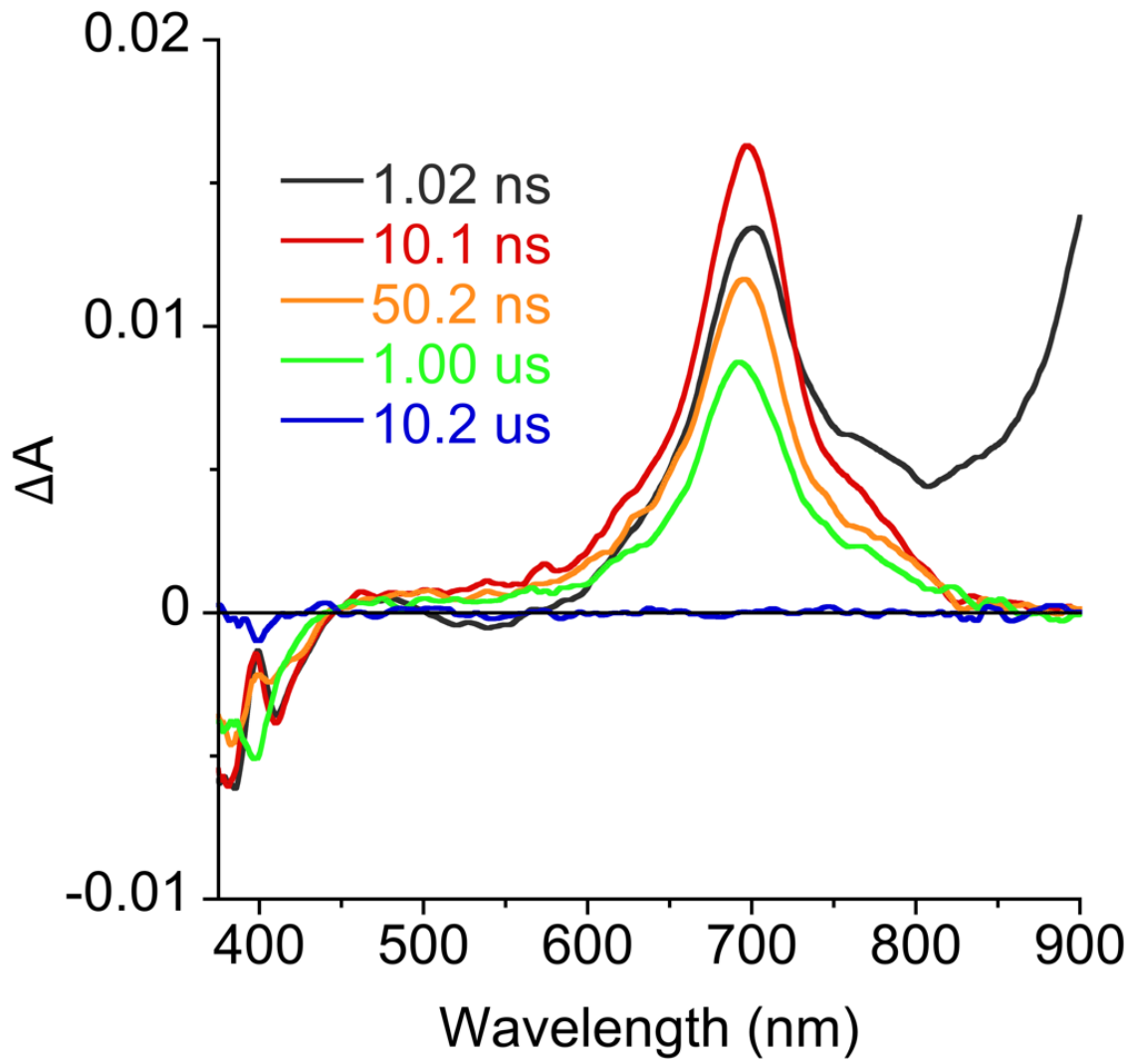

Figure 1.18: The T-T$_{max}$ absorption in OT6 extends into μs range.

spectra of T6DR appear similar to those of 1.4.(Figure 1.19) The first species after photoexcitation occurs within system response time and decays within 0.35 ps. It is a broad peak with $\lambda_{\max}$ at 670 nm. The second species, featuring two broad peaks near 550 and 850 nm, rises as the first species decays with a time constant of 193 ps.(Figure 1.19) The similarity in the transient absorption spectra of 1.4 and T6DR reveal that these two OTNN systems have similar electronic structures, i.e. excited electronic states configuration, regardless of the length or property of the OT precursors.

The excitation of T6DR with 650 nm light source generates the previously men-

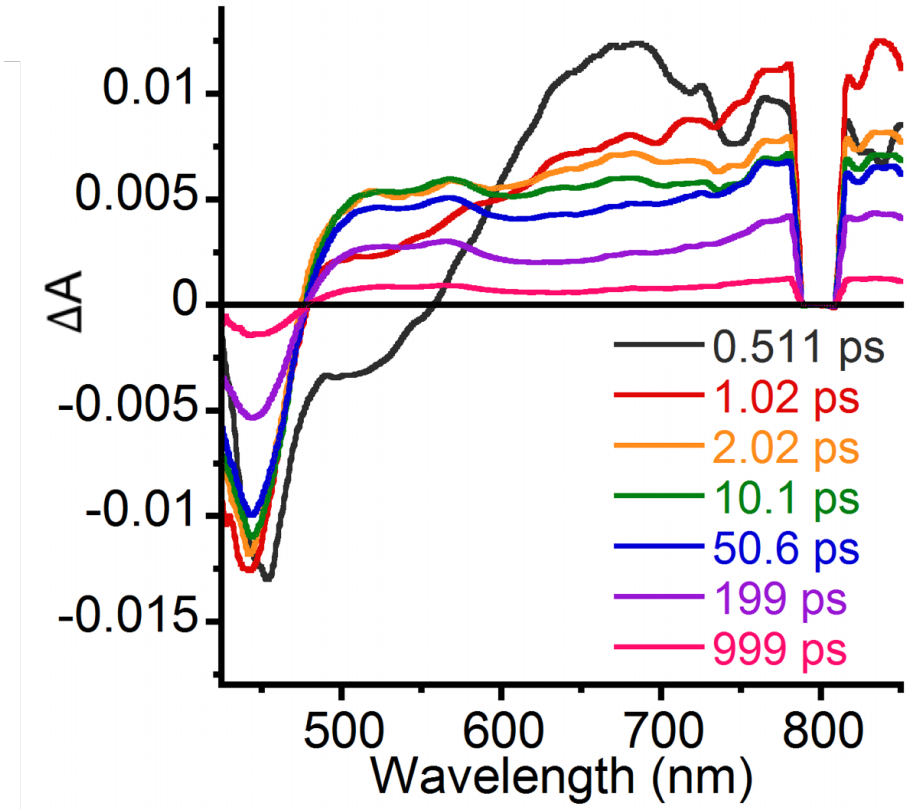

Figure 1.19: Time-resolved excited-state absorption spectra of T6DR with 400 nm excitation source. The first transient species has a 670 nm λ_{max} and is attributed to the absorption of S_H states. The second species features a broad absorption band with 550&850 nm λ_{max} and is attributed to the absorption of $S_C T$ states.

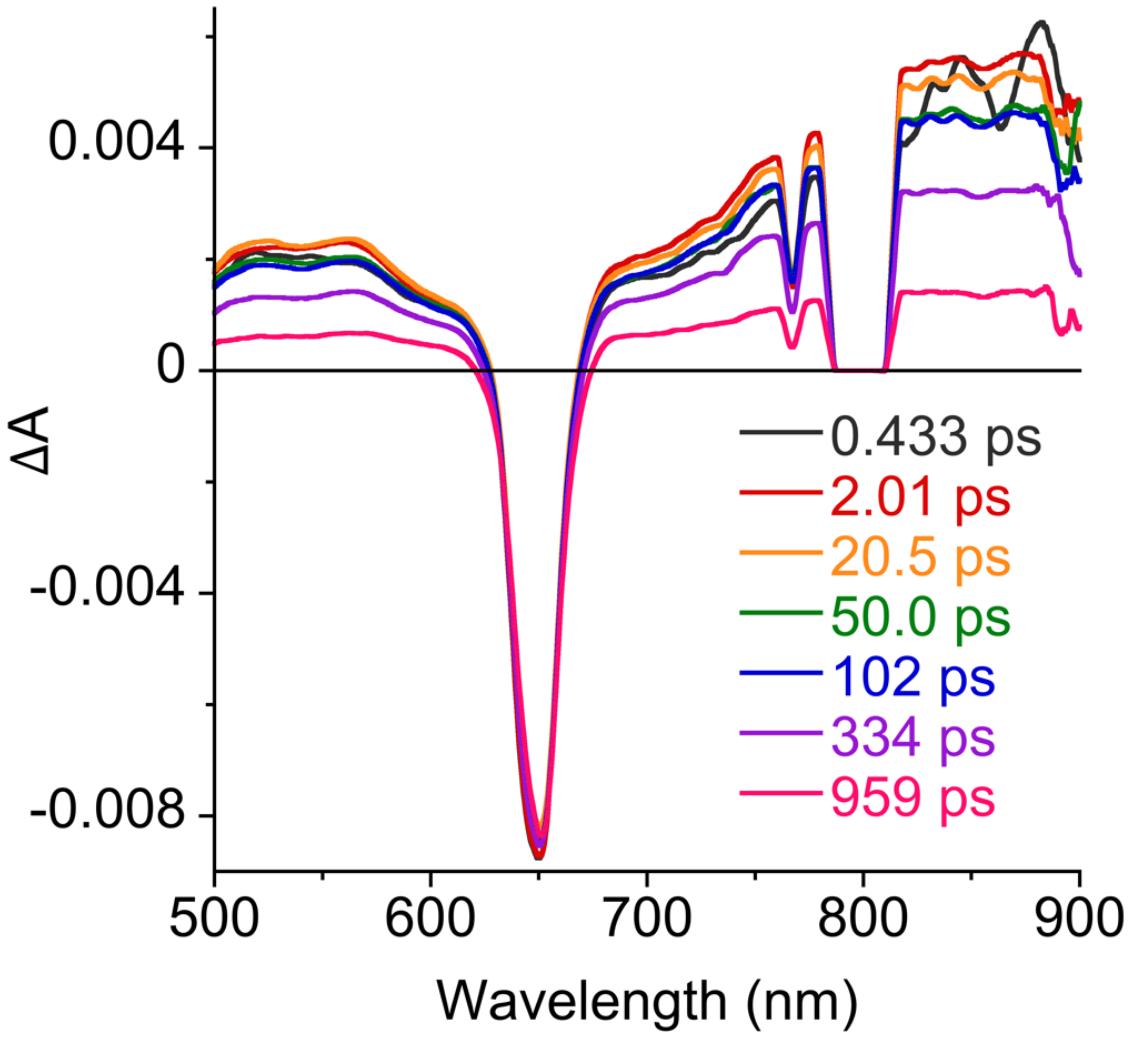

Figure 1.20: Time-resolved excited-state absorption spectra of T6DR with 650 excitation source. The only transient species generated by the 650 nm excitation source is S_{CT}, featuring a broad absorption band with 550&850 nm λ_{max}.

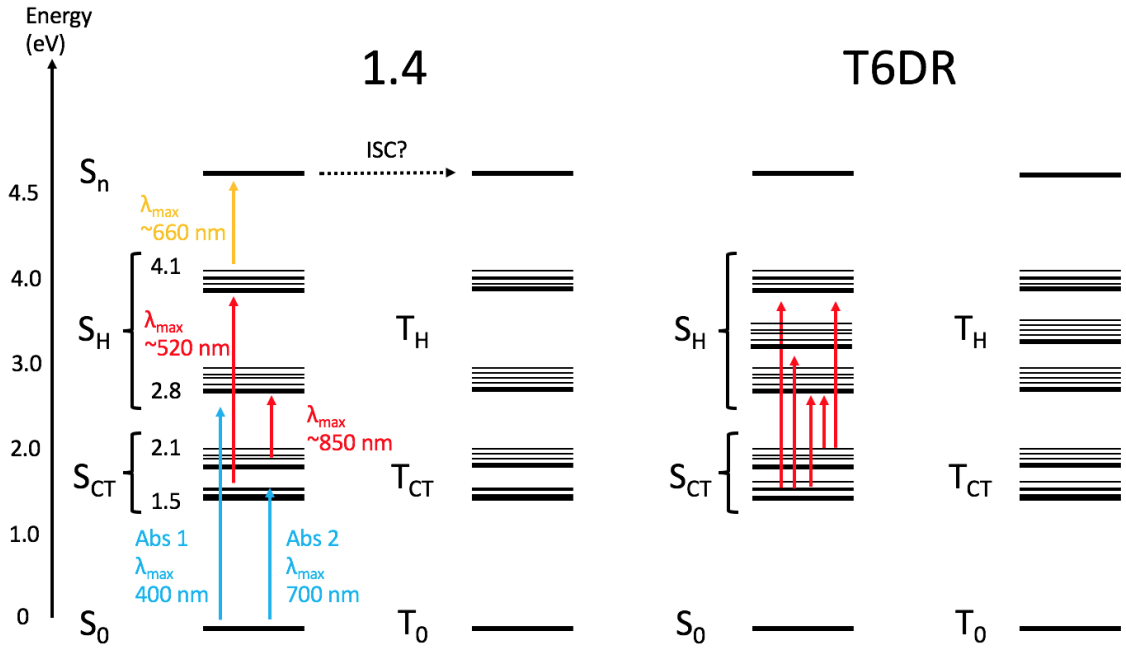

Figure 1.21: The electronic state configuration of 1.4 and T6DR. The blue arrows refer to ground state absorption. The yellow arrow refers to the absorption of the first transient species S_H. The red arrows refer to the absorption of the second species S_{CT} The multiple electronic states of similar energy are generated by spin-orbit coupling and the different combination of spin alignment. T6DR has more electrons than 1.4, so there are more electronic-state-splitting in T6DR. As a result, more transitions among electronic states are allowed, causing the broad absorption band. In theory, ISC should be faster in OTNN system than in OT, but no evidence of ISC is observed. Degenerate triplet states also exist and the same transition as in the singlet states take place. These transitions are omitted for clarity.

tioned second species with λ_{max} equal to 550 and 850 nm in the spectrum of T6DR with 400 nm excitation source. Since the 650 nm absorption peaks attribute to the n-π^* transition, which is a type of charge-transport transition, the species generated by 650 nm excitation source, i.e. the second species following 400 nm excitation, must have some degree of charge-transport-state character. So far the spectroscopic results have provided some information about the elusive electronic structures of oligothiophene-bis(nitronyl nitroxide) systems. In both 1.4 and T6DR, there lies a series of closely packed singlet excited states (S_H, H stands for Higher energy states) 2.8 4.1 eV (450-300 nm) above the ground state (S_0). There also exists a series of closely packed n-π^* induced charge-transport singlet states (S_{CT}) 1.5 2.1 eV (800-600 nm) above S_0. (Figure 1.21)

Upon excitation with a 650 nm laser, S_{CT} are populated before returning to S_0 within 1 ns. S_H are populated following a 400 nm excitation, and some of the excited state population decayed to ground state through IC and the rest moves to S_{CT}, which becomes populated as the signal of S_H vanishes. In 1.4, S_{CT} absorbs light of 2.4 eV (520 nm) and 1.5 eV (850 nm) as figure x indicates. These two values may correspond to the energy gap between S_{CT} and S_H, so the two absorptions should correspond to $S_{CT} \Rightarrow S_H$ transitions. The absorption band of S_{CT} in T6DR is much broader, referring to a larger number of similar-energy electronic states in T6DR than in 1.4. (Figure 1.21) This is because T6DR is a larger conjugated system than 1.4 and the spin-orbit coupling, which causes electronic-state-splitting, i.e. extra electronic states, is more dominant in T6DR. (Figure 1.21)

In the diradical systems, although the two excited states are noted as singlet states, they can also be triplet states, depending on the spin alignment on the two dangling radicals. (Figure 1.22)The radical spins can either have ferromagnetic or antiferromagnetic alignment, and the molecules with one of the alignment should have degenerate energy as the other since the magnetic interaction between the two

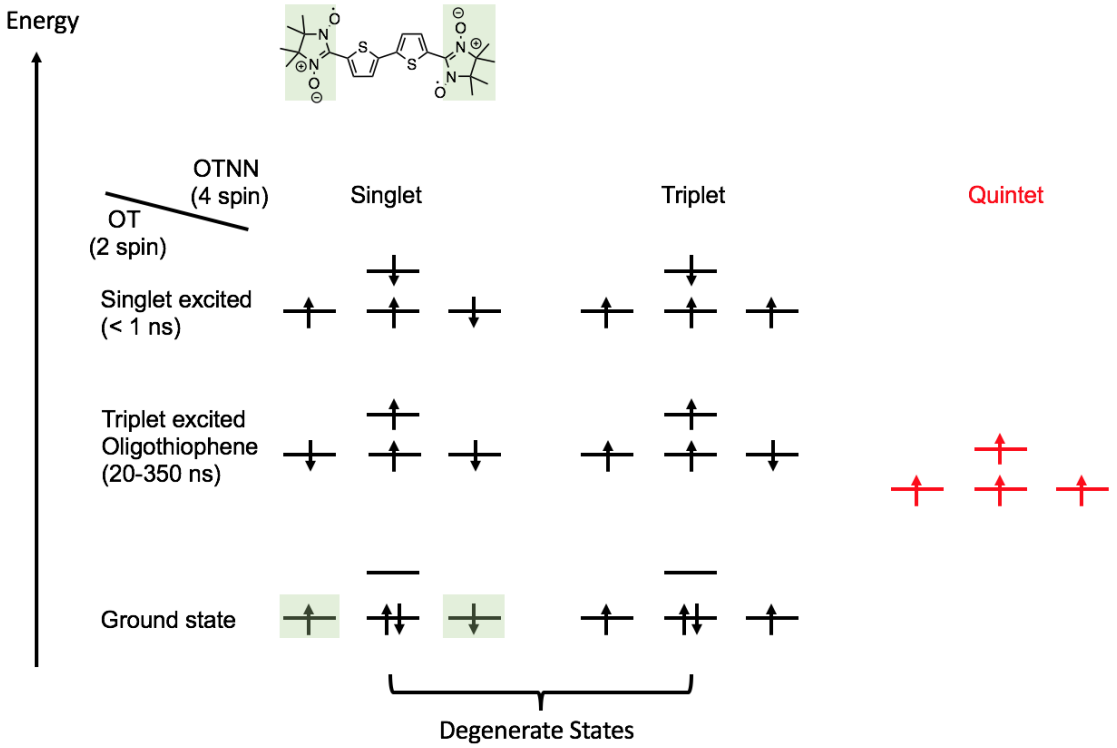

Figure 1.22: Degenerate singlet states and triplet states in the diradical systems. Quintet state may also exist, but is not observed.

radicals is small.[35] The degenerate radical spin alignments create a series of degenerate electronic states, which are further split by spin-orbit coupling.(Figure 1.22 1.21) The exact spin dynamics of the oligothiophene-radicals can be further studied by transient EPR.

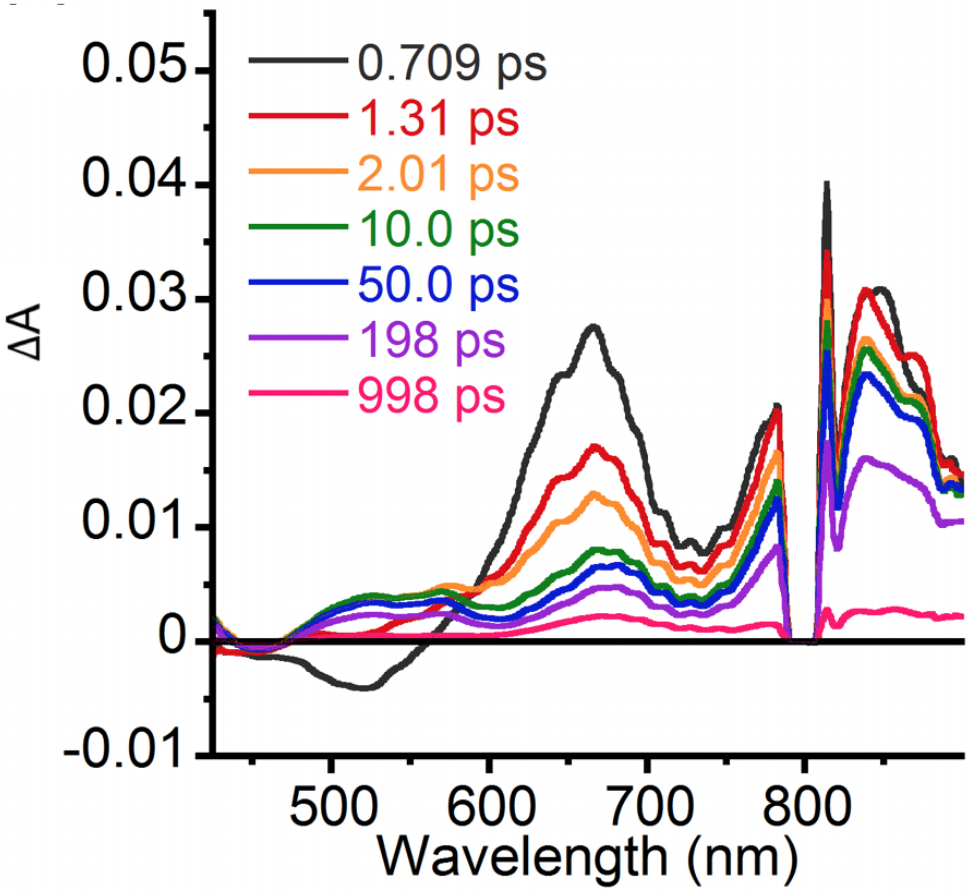

Figure 1.23: Time-resolved excited-state absorption spectra of 3.6. Two species constitute of D_H and D_{CT} are generated. The first species, dominated by D_H, has an emission at 525 nm and broad peaks with absorption maxima at 670 nm, 800 nm (predicted), and 850 nm. The second species is still dominated by D_H, but has some weak D_{CT} features near 500-550 nm.

Upon excitation with a 400 nm laser, 3.6 also generates two species. The first species has a lifetime of 1.1 ps, featuring three broad peaks with absorption maxima at 670 nm, 800 nm (predicted), and 850 nm.(Figure 1.25) The negative feature near 520 nm is caused by fluorescence. At first glance, the second species looks exactly the same as the first one. However, several small broad peaks in 480-550 nm range with intensity less than 0.005 ΔA rise following the decay of the first species. The lifetime of the second species is 577 ps. In 3.6, all existing states are either doublet or quartet configured because only three spins exist in the system.(Figure 1.24) Doublet states resemble the singlet states in diradical systems. Quartet, like quintet states,

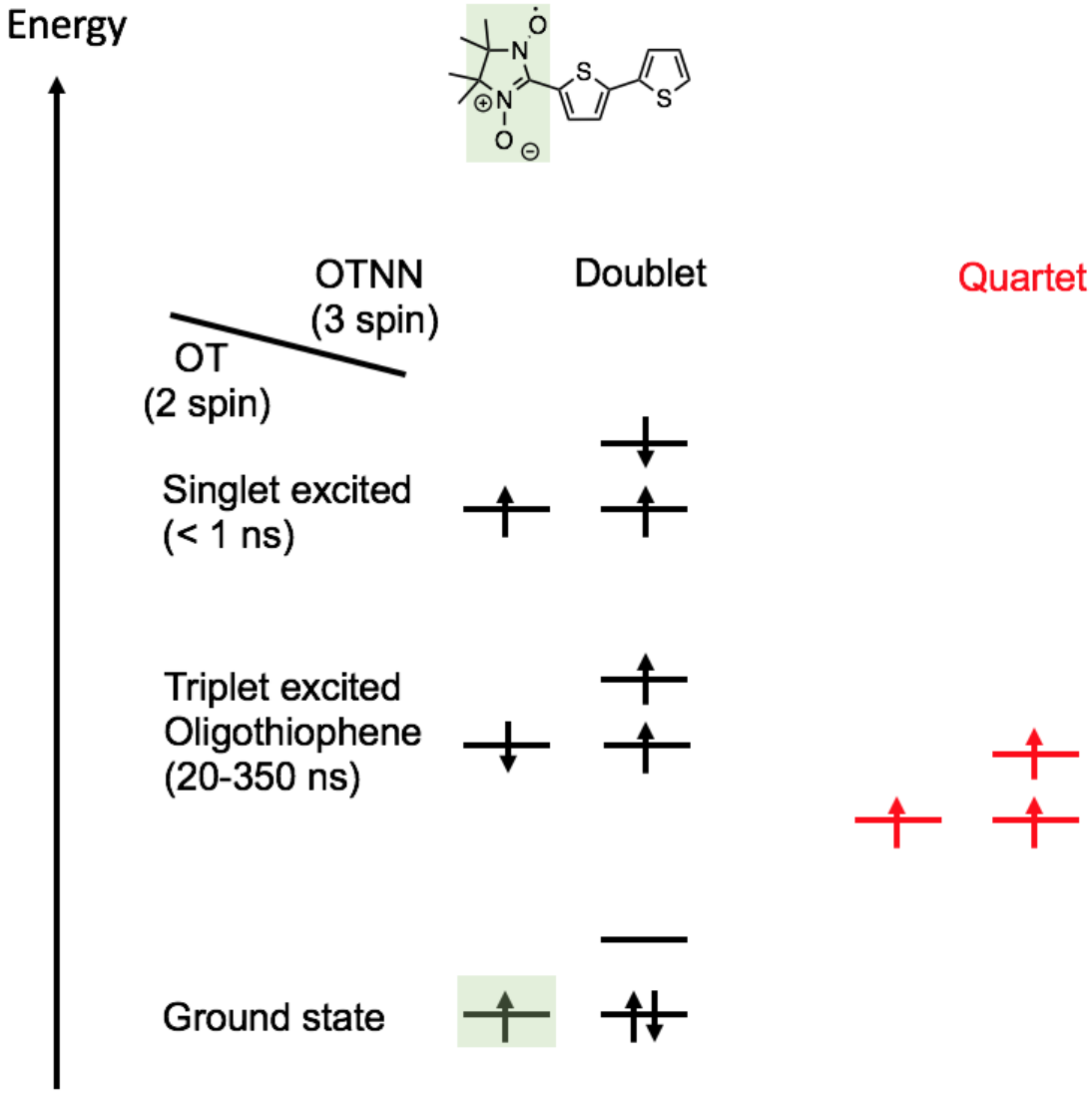

Figure 1.24: All electronic states are doublet or quartet configured because there are only three spins in the system. Doublet states resemble the singlet and triplet states in diradical systems. The quartet is not observed in experiments.

may exist in theory but its existence is not observed in experiments. Both species generated by photoexcitation are mixtures of D_H and D_{CT} states. In fact, the two species in 1.4 and T6DR are also mixtures. In both diradical (1.4, T6DR) and monoradical(3.6) systems, S_H is dominant in the first species, and S_{CT} feature is almost negligible. The second species in T6DR and 1.4 is predominantly S_{CT} and S_H feature is negligible as spin population goes to S_{CT} from S_H. In 3.6, however, D_H is still dominant in the second species, which makes its spectrum look almost identical to that of the first species. The second species has more D_H feature in 3.6 because the process of electrons/spins going from D_H to D_{CT} becomes more difficult as D_{CT} is weakened by the reduced number of radicals. Charge transfer (CT) states, i.e. S_{CT} and D_{CT}, states are generated by n-π^* transitions, which are proportional to the number of radicals in the system. The π^* refers to the coupled OT-NN molecular orbitals due to strong electronic interactions between OT and NN. As the number of radical decreases, the number of CT states also decreases, so fewer electrons can reside on CT states. In addition, according to Franck-Condon principle, the asymmetric geometry of 3.6 may increase the activation energy required for n-π^* transition, which infers increased difficulty in the process of electrons going from D_H to D_{CT}. A summary of the transient species is presented in Table 1.2.

Table 1.2: The optical properties of the transient species in OT2, OT6, 1.4, 3.6 and T6DR

cpd	λ_{max} 1 (nm)	τ_1 (ps)	λ_{max} 2 (nm)	τ_2 (ns)
OT2[33]	N\A	46	370	124000
OT6	620, 900	321 ± 29	710	1570 ± 30
1.4	667	0.201 ± 0.013	507, 834	0.161 ± 0.008
T6DR	670	0.346 ± 0.035	550, 850	0.193 ± 0.014
3.6	670, 800, 850	1.1 ± 0.04	500, 670,800,850	0.577 ± 0.028

Comparing the diradicals with the monoradical, the extra radical component in the former system extends the conjugation, creates C_2 symmetry, increases electronic coupling and generates a series of degenerate electronic states. These results all make transitions from ground states (S_0, D_0, or T_0) or non-CT excited states to CT states easier, signified by the higher 700 nm steady-state absorption intensity and weaker D_H feature in the second transient species following photoexcitation.

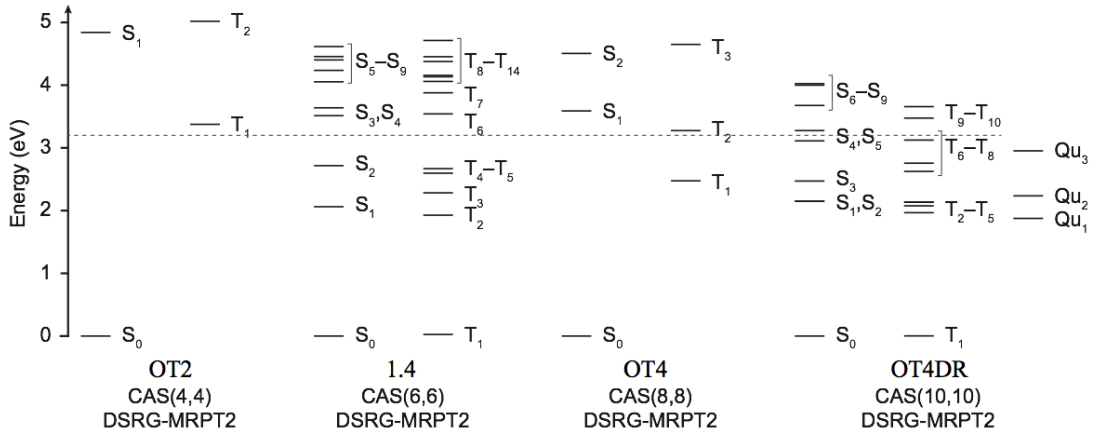

Figure 1.25: Computational approaches show the relative energies of the electronic states in OT2, 1.4, OT4 and T4DR.

1.3.7 Computation

Computation using DSRG-MRPT2 method, on the electronic structures of OT2, 1.4, tetrathiophene (OT4) and tetrathiophene-bis(nitronyl nitroxide) (T4DR) reveal that there are several extra singlet electronic states in the radicals lower than the original S1 of the non-radical oligothiophenes. The lowest-energy state(s) is/are S_{CT} and the ones about 2 eV higher in energy are S_H (S3, S4...) states. A set of triplet electronic states degenerate with the singlet states in the diradical systems is also presented, which confirms the degeneracy of the antiferromagnetic and ferromagnetic (radicals)spin alignment. Computation for T6DR and OT6 is not available because their sizes are beyond the limit of the method.

More detailed computations on T4DR show that its S_1, S_2 and T_4, T_5 states have charge-transfer features. Surprisingly, the charge-transfer is not a pure radical to oligothiophene-LUMO process. The electrons in the localized molecular orbitals of oligothiophene-chromophore, i.e. HOMO/HOMO-1/HOMO-2 (the first and second orbitals below HOMO) are able to transfer to the radical. Since T4DR shares similar structures with 1.4 and T6DR, the electronic-state compositions in the latter two

Table 1.3: The calculated compositions of each electronic state of T4DR (partial)

State	Energy (eV)	Configurations	Notes
S_0	0.00	$(\pi_{\text{HOMO-1}})^2(\pi_{\text{HOMO}})^2(r)^2$	R: 20, 02
S_1	2.15	15% $(\pi_{\text{HOMO-1}})^2(\pi_{\text{HOMO}})^1(r)^3$ + 15% $(\pi_{\text{HOMO-1}})^1(\pi_{\text{HOMO}})^2(r)^3$ + 14% $(\pi_{\text{HOMO-1}})^2(\pi_{\text{HOMO}})^2(r)^1(\pi_{\text{LUMO+1}})^1$ + 12% $(\pi_{\text{HOMO-1}})^2(\pi_{\text{HOMO}})^2(r)^1(\pi_{\text{LUMO}})^1$	
S_2	2.15	15% $(\pi_{\text{HOMO-1}})^1(\pi_{\text{HOMO}})^2(r)^3$ + 14% $(\pi_{\text{HOMO-1}})^2(\pi_{\text{HOMO}})^2(r)^1(\pi_{\text{LUMO+1}})^1$ + 12% $(\pi_{\text{HOMO-1}})^2(\pi_{\text{HOMO}})^2(r)^1(\pi_{\text{LUMO}})^1$ + 12% $(\pi_{\text{HOMO-1}})^2(\pi_{\text{HOMO}})^1(r)^3$ + 10% $(\pi_{\text{HOMO-2}})^1(\pi_{\text{HOMO-1}})^2(\pi_{\text{HOMO}})^2(r)^3$	
S_3	2.47	59% $(\pi_{\text{HOMO-1}})^2(\pi_{\text{HOMO}})^1(r)^2(\pi_{\text{LUMO}})^1$	R: aa, bb, ab, ba
S_4	3.11	73% $(\pi_{\text{HOMO-1}})^2(\pi_{\text{HOMO}})^1(r)^2(\pi_{\text{LUMO}})^1$	R: 20, 02 Corresponds to TTTT S_1
S_5	3.28	37% $(\pi_{\text{HOMO-1}})^2(\pi_{\text{HOMO}})^1(r)^2(\pi_{\text{LUMO+1}})^1$ + 25% $(\pi_{\text{HOMO-1}})^1(\pi_{\text{HOMO}})^2(r)^2(\pi_{\text{LUMO}})^1$	R: aa, bb, ab, ba
S_6	3.68	18% $(\pi_{\text{HOMO-1}})^2(\pi_{\text{HOMO}})^0(r)^2(\pi_{\text{LUMO}})^2$ + 11% $(\pi_{\text{HOMO-1}})^1(\pi_{\text{HOMO}})^2(r)^2(\pi_{\text{LUMO}})^1$ + 11% $(\pi_{\text{HOMO-1}})^2(\pi_{\text{HOMO}})^1(r)^2(\pi_{\text{LUMO+1}})^1$	R: 20, 02 (pi->pi*)
S_7	4.00	36% $(\pi_{\text{HOMO-1}})^2(\pi_{\text{HOMO}})^1(r)^2(\pi_{\text{LUMO+1}})^1$ + 29% $(\pi_{\text{HOMO-1}})^1(\pi_{\text{HOMO}})^2(r)^2(\pi_{\text{LUMO}})^1$	R: 20, 02 (pi->pi*)
S_8	4.02	7% $(\pi_{\text{HOMO-1}})^2(\pi_{\text{HOMO}})^1(r)^1(\pi_{\text{LUMO}})^2$ + 7% $(\pi_{\text{HOMO-1}})^1(\pi_{\text{HOMO}})^1(r)^3(\pi_{\text{LUMO}})^1$ + 7% $(\pi_{\text{HOMO-1}})^2(\pi_{\text{HOMO}})^0(r)^3(\pi_{\text{LUMO}})^1$	
S_9	4.02	7% $(\pi_{\text{HOMO-1}})^2(\pi_{\text{HOMO}})^1(r)^1(\pi_{\text{LUMO}})^2$ + 7% $(\pi_{\text{HOMO-1}})^1(\pi_{\text{HOMO}})^1(r)^3(\pi_{\text{LUMO}})^1$ + 6% $(\pi_{\text{HOMO-1}})^2(\pi_{\text{HOMO}})^0(r)^3(\pi_{\text{LUMO}})^1$	
T_1	0.00	83% $(\pi_{\text{HOMO-1}})^2(\pi_{\text{HOMO}})^2(r)^2$	R: ab, ba
T_2	1.97	54% $(\pi_{\text{HOMO-1}})^2(\pi_{\text{HOMO}})^1(r)^2(\pi_{\text{LUMO}})^1$ + 12% $(\pi_{\text{HOMO-1}})^1(\pi_{\text{HOMO}})^2(r)^2(\pi_{\text{LUMO+1}})^1$	R: 20, 02
T_3	2.08	40% $(\pi_{\text{HOMO-1}})^2(\pi_{\text{HOMO}})^1(r)^2(\pi_{\text{LUMO}})^1$ + 10% $(\pi_{\text{HOMO-1}})^1(\pi_{\text{HOMO}})^2(r)^2(\pi_{\text{LUMO+1}})^1$	R: aa, bb
T_4	2.13	15% $(\pi_{\text{HOMO-1}})^1(\pi_{\text{HOMO}})^2(r)^3$ + 13% $(\pi_{\text{HOMO-1}})^2(\pi_{\text{HOMO}})^2(r)^1(\pi_{\text{LUMO+1}})^1$ + 13% $(\pi_{\text{HOMO-1}})^2(\pi_{\text{HOMO}})^2(r)^1(\pi_{\text{LUMO}})^1$ + 12% $(\pi_{\text{HOMO-1}})^2(\pi_{\text{HOMO}})^1(r)^3$	
T_5	2.13	14% $(\pi_{\text{HOMO-1}})^1(\pi_{\text{HOMO}})^2(r)^3$ + 13% $(\pi_{\text{HOMO-1}})^2(\pi_{\text{HOMO}})^2(r)^1(\pi_{\text{LUMO+1}})^1$ + 13% $(\pi_{\text{HOMO-1}})^2(\pi_{\text{HOMO}})^2(r)^1(\pi_{\text{LUMO}})^1$ + 12% $(\pi_{\text{HOMO-1}})^2(\pi_{\text{HOMO}})^1(r)^3$	

should be the same. Therefore, the charge-transfer character of the i.e. S_{CT} and T_{CT} states are confirmed by computational approaches.

1.4 Conclusion

Bithiophene-bis(nitronyl nitroxide) (1.4) and sexithiophene-mono-nitronyl nitroxide (3.6) have been synthesized successfully. Their structures have been confirmed with ESI-MS. EPR spectra of 1.4 show strong HFT signal, which demonstrates the high purity of the sample, along with intramolecular electron-electron interaction. Parallel-displaced π-stacking have been found to be the driving force for the crystal formation of 1.4. The red-shifted steady-state absorption spectra show that OTNN systems have lower bandgap than the corresponding oligothiophene, which is caused by the strong electronic coupling between the molecular orbitals of oligothiophene chromophore and the radical(s). The degree of red-shift, i.e. electronic coupling, is positively correlated with the number of radicals. Fluorescence quenching and triplet quenching are observed in all the radicals discussed, and they are partially caused by the presence of S_{CT} (and degenerate T_{CT}) in between S_H and S_0. IC is the other reason for fluorescence and triplet quenching. Computational approaches have suggested the charge-transport nature of S_{CT} and the presence of a set of triplet states degenerate to the singlet states. The studies presented in this thesis have set the foundations for further analysis on the spin-dynamics of oligothiophene-radical systems. Once the detailed post-photoexcitation transitions are known, modification on the molecular structure, such as extending or disrupting conjugation, can be made in order to optimize the optical and correlated magnetic properties of the oligothiophene-radical systems.

Appendix A Appendix

A.1 Appendix section

Crystal data and structure refinement for 1.4.

Identification code	1.4
Empirical formula	$C_{22}H_{28}N_4O_4S_2$
Formula weight	476.60
Temperature/K	100(2)
Crystal system	triclinic
Space group	P-1
a/Å	8.6033(19)
b/Å	11.704(3)
c/Å	12.974(4)
α/°	67.750(3)
β/°	76.075(4)
γ/°	70.501(3)
Volume/Å^3	1129.9(5)
Z	2
ρ_{calc}g/cm^3	1.401
μ/mm^{-1}	0.273
F(000)	504.0
Crystal size/mm^3	0.359 × 0.313 × 0.104
Radiation	MoKα (λ = 0.71073)
2Θ range for data collection/°	3.422 to 58.31
Index ranges	$-11 \leq h \leq 11$, $-16 \leq k \leq 16$, $-17 \leq l \leq 17$
Reflections collected	11992
Independent reflections	6044 [R_{int} = 0.0951, R_{sigma} = 0.3524]
Data/restraints/parameters	6044/45/297
Goodness-of-fit on F^2	0.953
Final R indexes [I>=2σ (I)]	R_1 = 0.0644, wR_2 = 0.1305
Final R indexes [all data]	R_1 = 0.1198, wR_2 = 0.1496
Largest diff. peak/hole / e Å^{-3}	0.62/-0.39

Table A.1: Crystal information of 1.4

Table A.2: The calculated compositions of each electronic state of T4DR (second half)

T_6	2.62	26% $(\pi_{\text{HOMO-1}})^2(\pi_{\text{HOMO}})^1(r)^2(\pi_{\text{LUMO}})^1$ + 26% $(\pi_{\text{HOMO-1}})^2(\pi_{\text{HOMO}})^1(r)^2(\pi_{\text{LUMO+2}})^1$	R: aa, bb. aa, bb, ab, ba
T_7	2.76	13% $(\pi_{\text{HOMO-1}})^2(\pi_{\text{HOMO}})^1(r)^2(\pi_{\text{LUMO+1}})^1$ + 12% $(\pi_{\text{HOMO-1}})^1(\pi_{\text{HOMO}})^2(r)^2(\pi_{\text{LUMO}})^1$ + 15% $(\pi_{\text{HOMO}})^2(\pi_{\text{HOMO}})^1(r)^2(\pi_{\text{LUMO+2}})^1$ + 13% $(\pi_{\text{HOMO}})^2(\pi_{\text{HOMO}})^1(r)^2(\pi_{\text{LUMO}})^1$	R: aa, bb. aa, bb. 20, 02. 20, 02.
T_8	3.12	73% $(\pi_{\text{HOMO-1}})^2(\pi_{\text{HOMO}})^1(r)^2(\pi_{\text{LUMO}})^1$	R: ab, ba
T_9	3.47	12% $(\pi_{\text{HOMO-1}})^2(\pi_{\text{HOMO}})^1(r)^2(\pi_{\text{LUMO+1}})^1$ + 8% $(\pi_{\text{HOMO-1}})^1(\pi_{\text{HOMO}})^2(r)^2(\pi_{\text{LUMO}})^1$	R: aa, bb. aa, bb.
T_{10}	3.66	13% $(\pi_{\text{HOMO-1}})^2(\pi_{\text{HOMO}})^1(r)^2(\pi_{\text{LUMO+1}})^1$ + 11% $(\pi_{\text{HOMO-1}})^2(\pi_{\text{HOMO}})^1(r)^2(\pi_{\text{LUMO+3}})^1$	R: 20, 02. 20, 02
Qu_1	1.88	64% $(\pi_{\text{HOMO-1}})^2(\pi_{\text{HOMO}})^1(r)^2(\pi_{\text{LUMO}})^1$ + 14% $(\pi_{\text{HOMO-1}})^1(\pi_{\text{HOMO}})^2(r)^2(\pi_{\text{LUMO+1}})^1$	R: aa, bb, ab, ba
Qu_2	2.24	36% $(\pi_{\text{HOMO-1}})^2(\pi_{\text{HOMO}})^1(r)^2(\pi_{\text{LUMO+1}})^1$ + 35% $(\pi_{\text{HOMO-1}})^1(\pi_{\text{HOMO}})^2(r)^2(\pi_{\text{LUMO}})^1$	R: aa, bb, ab, ba
Qu_3	2.95	25% $(\pi_{\text{HOMO-1}})^2(\pi_{\text{HOMO}})^1(r)^2(\pi_{\text{LUMO+2}})^1$ + 23% $(\pi_{\text{HOMO-2}})^1(\pi_{\text{HOMO}})^2(r)^2(\pi_{\text{LUMO}})^1$ + 21% $(\pi_{\text{HOMO-1}})^1(\pi_{\text{HOMO}})^2(r)^2(\pi_{\text{LUMO+1}})^1$	R: aa, bb, ab, ba
Qu_4	3.88	19% $(\pi_{\text{HOMO-2}})^1(\pi_{\text{HOMO}})^2(r)^2(\pi_{\text{LUMO+1}})^1$ + 18% $(\pi_{\text{HOMO-1}})^2(\pi_{\text{HOMO}})^1(r)^2(\pi_{\text{LUMO+1}})^1$ + 18% $(\pi_{\text{HOMO-3}})^1(\pi_{\text{HOMO}})^2(r)^2(\pi_{\text{LUMO}})^1$ + 15% $(\pi_{\text{HOMO-1}})^2(\pi_{\text{HOMO}})^1(r)^2(\pi_{\text{LUMO+3}})^1$ + 11% $(\pi_{\text{HOMO-1}})^1(\pi_{\text{HOMO}})^2(r)^2(\pi_{\text{LUMO+2}})^1$	R: aa, bb, ab, ba

Bibliography

(1) Wolf, S. A.; Awschalom, D. D.; Buhrman, R. A.; Daughton, J. M.; von Molnár, S.; Roukes, M. L.; Chtchelkanova, A. Y.; Treger, D. M. *Science* **2001**, *294*, 1488–1495.

(2) Awschalom, D. D.; Flatte, M.; Samarth, N. *Sci. Am.* **2002**, *286*, 67.

(3) Rajca, A. *Chem. Rev.* **1994**, *94*, 871–893.

(4) Chen, F.; Chen, F.; Koufaty, D. a.; Koufaty, D. a.; Zhang, X.; Zhang, X. *Perf. E. R. Si.* **2009**, *37*, 181–192.

(5) Gary Prinz, A. *Science* **1998**, *282*, 1660–1663.

(6) Prinz, G. a. *Science* **1997**, *1997*, 1660–1663.

(7) Deng, D.-L.; Li, X.; Sarma, S. D. *arXiv preprint arXiv:1701.04844* **2017**.

(8) Xiang, H.; Shi, F. Y.; Zhang, C.; Rzchowski, M. S.; Voyles, P. M.; Chang, Y. A. *Scripta Materialia* **2011**, *65*, 739–742.

(9) Shi, F.; Xiang, H.; Yang, J. J.; Rzchowski, M. S.; Chang, Y. A.; Voyles, P. M. *J. Magn. Magn. Mater* **2012**, *324*, 1837–1844.

(10) Ueda, K.; Tabata, H.; Kawai, T. *Appl. Phys. Lett.* **2001**, *79*, 988–990.

(11) Giacobbe, E. M.; Mi, Q.; Colvin, M. T.; Cohen, B.; Ramanan, C.; Scott, M.; Yeganeh, S.; Marks, T. J.; Ratner, M. A.; Wasielewski, M. R.; Scott, A. M. *J. Am. Chem. Soc.* **2009**, 3700–3712.

(12) Kawanaka, Y.; Shimizu, A.; Shinada, T.; Tanaka, R.; Teki, Y. *Angewandte Chemie - International Edition* **2013**, *52*, 6643–6647.

(13) Teki, Y.; Miyamoto, S.; Nakatsuji, M.; Miura, Y. *J. Am. Chem. Soc* **2001**, *123*, 294–305.

(14) Takeuchi, S.; Ishii, K.; Kobayashi, N. *J. Phys. Chem. A* **2004**, *108*, 3276–3280.

(15) Ito, A.; Shimizu, A.; Kishida, N.; Kawanaka, Y.; Kosumi, D.; Hashimoto, H.; Teki, Y. *Angewandte Chemie - International Edition* **2014**, *53*, 6715–6719.

(16) Colvin, M. T.; Giacobbe, E. M.; Cohen, B.; Miura, T.; Scott, A. M.; Wasielewski, M. R. *J. Phys. Chem. A* **2010**, *114*, 1741–1748.

(17) Green, S.; Fox, M. A. *J. Phys. Chem.* **1995**, *99*, 14752–14757.

(18) Yee, W. A.; Kuzmin, V.; Kliger, D. S.; Hammond, G. S.; A.J., T. *J. Am. Chem. Soc.* **1979**, *101*, 5104–5106.

(19) Herbelin, S. E.; Blough, N. V. *J. Phys. Chem. B* **1998**, *102*, 8170–8176.

(20) Armour, M.; Davies, A. G.; Upadhyay, J.; Wassermann, A. *J. Polym. Sci. A1* **1967**, *5*, 1527–1538.

(21) Kojmehl, G.; Chatzitheodorou, G. *Makromol. Chem-Rapid* **1981**, *555*, 551–555.

(22) Tourillon, G.; Garnier, F. *Thin Solid Films* **1983**, *2*, 287–403.

(23) Kaneto, K.; Yoshino, K.; Inuishi, Y. *Jpn. J. Appl. Phys.* **1983**, *22*, L412.

(24) Tada, K.; Harada, H.; Yoshino, K. *Jpn. J. Appl. Phys* **1996**, *35*, 944–946.

(25) McCullough, R. D. *Adv. Mater.* **1998**, *10*, 93–116.

(26) Williams, S. P.; t Renae, D. L. *J. Am. Chem. Soc* **1993**, *115*, 1.

(27) Rittmeyer, S. P.; Groß, A. *Beilstein J. Nanotechnol* **2012**, *3*, 909–919.

(28) Beljonne, D.; Cornil, J.; Friend, R. H.; Janssen, R. A. J.; Brédas, J. L. *J. Am. Chem. Soc* **1996**, *118*, 6453–6461.

(29) Camarada, M. B.; Jaque, P.; Díaz, F. R.; del Valle, M. A. *J. Polym. Sci. Pol. Phys.* **2011**, *49*, 1723–1733.

(30) Bucella, S. G.; Luzio, A.; Gann, E.; Thomsen, L.; McNeill, C. R.; Pace, G.; Perinot, A.; Chen, Z.; Facchetti, A.; Caironi, M. *Nat. Commun.* **2015**, *6*, 8394.

(31) Fujitsuka, M.; Ito, O.; Yamashiro, T.; Aso, Y.; Otsubo, T. *J. Phys. Chem. A* **2000**, *104*, 4876–4881.

(32) Horowitz, G.; Garnier, F.; Yassar, A.; Hajlaoui, R.; Kouki, F. *Adv. Mater.* **1996**, *8*, 52–54.

(33) Becker, R. S.; Seixas De Melo, J.; Maçanita, A. L.; Elisei, F. *J. Phys. Chem.* **1996**, *100*, 18683–18695.

(34) Aydın, M.; Esat, B.; Kılıç, Ç.; Köse, M. E.; Ata, A.; Yılmaz, F. *Eur. Polym. J.* **2011**, *47*, 2283–2294.

(35) Mitsumori, T.; Inoue, K.; Koga, N.; Iwamura, H. *J. Am. Chem. Soc.* **1995**, *117*, 2467–2478.

(36) Dolomanov, O. V.; Bourhis, L. J.; Gildea, R. J.; Howard, J. A. K.; Puschmann, H. *J. Appl. Crystallogr.* **Apr. 2009**, *42*, 339–341.

(37) Sheldrick, G. M. *Acta Cryst.* **2015**, *A71*, 3–8.

(38) Sheldrick, G. M. *Acta Cryst.* **2008**, *A64*, 112–122.

(39) Bader, M. M.; Pham, P.-T. T.; Elandaloussi, E. H. *Cryst. Growth Des.* **2010**, *10*, 5027–5030.

(40) Rajca, A.; Pink, M.; Mukherjee, S.; Rajca, S.; Das, K. *Tetrahedron* **2007**, *63*, 10731–10742.

(41) Hirel, C.; Vostrikova, K. E.; Pécaut, J.; Ovcharenko, V. I.; Rey, P. *Chem-Eur J.* **2001**, *7*, 2007–2014.

(42) Borozdina, Y. B.; Mostovich, E. a.; Enkelmann, V.; Wolf, B.; Cong, P. T.; Tutsch, U.; Lang, M.; Baumgarten, M. *J. Mater. Chem. C* **2014**, *2*, 6618–6629.

(43) Bhuwalka, A.; Mike, J. F.; He, M.; Intemann, J. J.; Nelson, T.; Ewan, M. D.; Roggers, R. A.; Lin, Z.; Jeffries-EL, M. *Macromolecules* **2011**, *44*, 9611–9617.

(44) Osiecki, J. H.; Ullman, E. F. *J. Am. Chem. Soc* **1968**, *90*, 1078–1079.

(45) Tretyakov, E.; Okada, K.; Suzuki, S.; Baumgarten, M.; Romanenko, G.; Bogomyakov, A.; Ovcharenko, V. *J. Phys. Org. Chem.* **2016**, *29*, POC-15-0239.R1, 725–734.

(46) Würth, C.; Grabolle, M.; Pauli, J.; Spieles, M.; Resch-genger, U. *Nat. Protoc.* **2013**, *8*, 1535–50.